Journal of Mathematical Imaging and Vision 21: 135–154, 2004

Euclidean Group Invariant Computation of Stochastic Completion Fields Using Shiftable-Twistable Functions

JOHN ZWECK
Department of Mathematics and Statistics, University of Maryland Baltimore County, Baltimore, MD 21250, USA
zweck@umbc.edu

LANCE R. WILLIAMS
Department of Computer Science, University of New Mexico, Albuquerque, NM 87131, USA
williams@cs.unm.edu

Abstract. We describe a method for computing the likelihood that a completion joining two contour fragments passes through any given position and orientation in the image plane. Like computations in primary visual cortex (and unlike all previous models of contour completion), the output of our computation is invariant under rotations and translations of the input pattern. This is achieved by representing the input, output, and intermediate states of the computation in a basis of shiftable-twistable functions.

Keywords: boundary completion, Euclidean invariant computation, visual cortex, shiftable basis, Fokker-Planck equation

1. Introduction

Any computational model of human visual information processing must reconcile two apparently contradictory observations. First, contour computations in primary visual cortex are *Euclidean invariant*—small rotations and translations of the input pattern of light falling on the retina produce identical rotations and translations of the output of the computation. Second, simple calculations based on the size of primary visual cortex (60 mm $\times$ 80 mm) and the observed density of cortical hypercolumns (4/mm^2) suggest that the discrete spatial sampling of the visual field is exceedingly sparse [16]. The apparent contradiction becomes clear when we ask the following questions: How is this remarkable invariance achieved in computations performed by populations of cortical neurons with broadly tuned receptive fields centered at so few locations? Why doesn't our perception of the world change dramatically when we tilt our head by 5 degrees?

One of the main goals of our research is to show how the sparse sampling of the visual field can be reconciled with the local Euclidean invariance of visual computations. To realize this goal, we introduce the notion of a shiftable-twistable basis of functions on the space, $\mathbf{R}^2 \times S^1$, of positions and directions. This notion is a generalization of the notion of a shiftable-steerable basis of functions on the plane, $\mathbf{R}^2$, introduced by Freeman, Adelson, Simoncelli, and Heeger in two seminal papers [4, 14]. Freeman and Adelson [4] clearly appreciated the importance of the issues raised above when they devised the notion of a steerable basis to implement rotationally invariant computations. In fact, for computations in the plane the contradictions discussed above were largely resolved with the introduction by Simoncelli et al. [14] of the shiftable-steerable pyramid transform, which was specifically designed to perform Euclidean invariant computations on $\mathbf{R}^2$. The basis functions in the shiftable-steerable pyramid are very similar to simple cell receptive fields in primary visual cortex. However, many computations in visual cortex likely operate on functions on the space of positions and directions, $\mathbf{R}^2 \times S^1$, rather than on functions on the plane, $\mathbf{R}^2$ (e.g.

[5, 6, 8, 10, 12, 17, 18, 22]). Consequently, we propose that shiftability-twistability (in addition to shiftability-steerability) is the property which binds sparsely distributed receptive fields together functionally to perform Euclidean invariant computations in visual cortex.

In this article, we describe a new algorithm for completing the boundaries of partially occluded objects. This algorithm is based on a computational theory of contour completion in primary and secondary visual cortex developed in recent years by Williams and colleagues [15, 17–19]. Like computations in visual cortex, and unlike previous models of illusory contour formation, our computation is Euclidean invariant. This invariance is achieved by representing the input, output, and intermediate states of the computation in a basis of shiftable-twistable functions.

Mumford [9] proposed that the probability distribution of natural shapes can be modeled by particles traveling with constant speed in directions given by Brownian motions. More recently, Williams and Jacobs [17] defined the *stochastic completion field* to be the distribution of particle trajectories joining pairs of position and direction constraints, and showed how it could be computed in a neural network.

The neural network described in [18] is based on Mumford's observation that the evolution in time of the probability density function (p.d.f.) representing the position, (x, y), and direction, θ, of a particle can be modeled as a set of independent advection equations acting in the (x, y) dimension coupled in the θ dimension by the diffusion equation [9]. Unfortunately, solutions of this *Fokker-Planck* equation computed by numerical integration on a rectangular grid do not exhibit the robust invariance under small rotations and translations which characterizes the output of computations performed in primary visual cortex. Nor does any other existing model of contour completion, sharpening, or saliency ([e.g. 5, 6, 8, 10, 12, 17, 18, 22]).

Our new algorithm computes stochastic completion fields in a Euclidean invariant manner. Figure 2 (left) is a picture of the stochastic completion field due to the Kanizsa Triangle stimulus in Fig. 1(b). Figure 2 (right) shows the stochastic completion field due to a rotation and translation of the (input) Kanizsa Triangle. The Euclidean invariance of our algorithm can be seen by observing that the (output) stochastic completion field on the right in Fig. 2 is itself a rotation and translation of the stochastic completion field on the left, by the same amount.

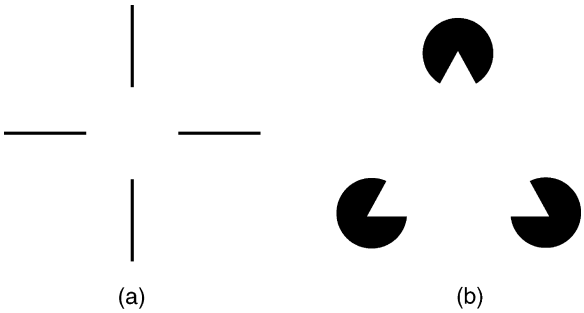

Figure 1. (a) Ehrenstein figure. (b) Kanizsa triangle.

In subsequent work [20], we have extended the results presented here and in [19] by describing a discrete neural network that enhances and completes salient *closed* contours in a shift-twist invariant manner. Like the input provided to primary visual cortex by the lateral geniculate nucleus, the input to the computation in [20] is isotropic. That is, it is composed of spots, not edges.

Euclidean invariance is a property only of computations defined in the continuum. However, we will show that certain Euclidean invariant computations in the continuum can be implemented using a finite number of operations on a finite number of basis functions, provided that the discrete implementation of the continuous computation is carefully designed to preserve Euclidean invariance. The general approach we adopt in this paper involves explicitly using the shiftability and twistability of the basis functions to transform a Euclidean invariant computation in the continuum into a discrete computation on a lattice. The discrete computation operates on the coefficients of a wavelet-like transform of the function to be computed. This approach to visual computations is in accord with the hypothesis of Daugman [3] (and others, e.g. [7, 11]) that an ensemble of simple cell receptive fields can be regarded as performing a wavelet transform of the image, in which the responses of the neurons correspond to the transform coefficients and the receptive fields correspond to the basis functions. Further biological motivation for our approach can be found in [20].

2. Shiftable-Twistable Bases

Many visual and image processing tasks are most naturally formulated in the continuum and are invariant under a group of symmetries of the continuum. The

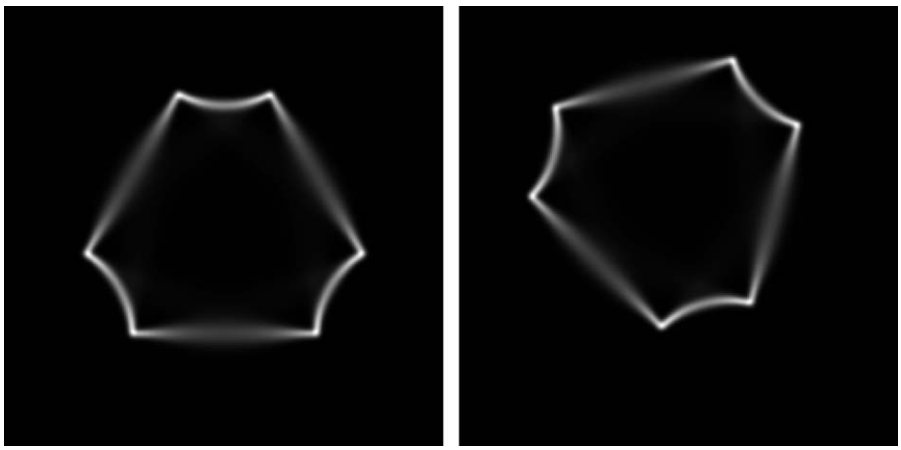

Figure 2. Stochastic completion fields. Left: Of Kanizsa triangle. Right: After the initial conditions have been rotated and translated.

Euclidean group, of rotations and translations, is one example of a continuous symmetry group. However, because discrete lattices are not preserved by the action of continuous symmetry groups, the natural invariance of a computation can be easily lost when it is performed in a discrete network. In this section we will introduce the notion of a shiftable-twistable basis and show how it can be used to implement discrete computations on the continuous space of positions and directions in a way which preserves their natural invariance.

In image processing, the input and output are functions on $\mathbf{R}^2$, and the appropriate notion of the invariance of computations is *Euclidean invariance*—any rotation and translation of the input should produce an identical rotation and translation of the output. Simoncelli et al. [14] and Freeman and Adelson [4] introduced the notion of a shiftable-steerable basis of functions on $\mathbf{R}^2$, and showed how it can be used to achieve Euclidean invariance in discrete computations for image enhancement, stereo disparity measurement, and scale-space analysis.

Given the nature of simple cell receptive fields, the input and output of computations in primary visual cortex are more naturally thought of as functions defined on the continuous space, $\mathbf{R}^2 \times S^1$, of positions, $\vec{x} = [x, y]^T$, in the plane, $\mathbf{R}^2$, and directions, θ, in the circle, S^1. For such computations the appropriate notion of invariance is determined by those symmetries, $T_{\vec{x}_0,\theta_0}$, of $\mathbf{R}^2 \times S^1$, which perform a shift in $\mathbf{R}^2$ by $\vec{x}_0$, followed by a twist in $\mathbf{R}^2 \times S^1$ through an angle, θ_0. A *twist* through an angle, θ_0, consists of two parts: (1) a rotation, R_{θ_0}, of $\mathbf{R}^2$ and (2) a translation in S^1, both by θ_0. The symmetry, $T_{\vec{x}_0,\theta_0}$, which is called a *shift-twist transformation*, is given by the formula,

$$T_{\vec{x}_0,\theta_0}(\vec{x},\theta) = \big(R_{\theta_0}(\vec{x} - \vec{x}_0)\,,\ \theta - \theta_0\big). \tag{2.1}$$

The relationship between continuous shift-twist transformations and computations in primary visual cortex was first hypothesized by Williams and Jacobs [17], who observed that the continuous shift-twist group characterized the symmetry of the Green's function of the Fokker-Planck equation[1] described by Mumford [9]:

$$G(\vec{x},\theta;t_1 \mid \vec{u},\phi;t_0) = G(T_{\vec{u},\phi}(\vec{x},\theta);t_1 - t_0 \mid 0,0;0).$$

The shift-twist of a complex-valued[2] function, $P : \mathbf{R}^2 \times S^1 \to \mathbf{C}$, on $\mathbf{R}^2 \times S^1$ by an amount, $(\vec{x}_0,\theta_0) \in \mathbf{R}^2 \times S^1$, is the function, $T_{\vec{x}_0,\theta_0}P : \mathbf{R}^2 \times S^1 \to \mathbf{C}$, defined by

$$\big(T_{\vec{x}_0,\theta_0}P\big)(\vec{x},\theta) = P\big(T_{\vec{x}_0,\theta_0}(\vec{x},\theta)\big). \tag{2.2}$$

A visual computation on $\mathbf{R}^2 \times S^1$ is called *shift-twist invariant* if, for all $(\vec{x}_0,\theta_0) \in \mathbf{R}^2 \times S^1$, a shift-twist of the input function by $(\vec{x}_0,\theta_0)$ produces an identical shift-twist of the output function. Correspondingly, we define a *shiftable-twistable basis*[3] of functions on $\mathbf{R}^2 \times S^1$ to be a set of functions with the property that whenever a function, $P : \mathbf{R}^2 \times S^1 \to \mathbf{C}$, is in their span, then so is $T_{\vec{x}_0,\theta_0}P$, for every choice of $(\vec{x}_0,\theta_0)$ in $\mathbf{R}^2 \times S^1$. As such, the notion of a shiftable-twistable basis on $\mathbf{R}^2 \times S^1$ generalizes that of a shiftable-steerable basis on $\mathbf{R}^2$.

Shiftable-twistable bases can be constructed as follows. First we recall Simoncelli's concept of the shiftability of a function, which is closely related to the Shannon-Whittaker Sampling Theorem. A periodic function, $\psi : \mathbf{R} \to \mathbf{C}$, of period X, is *shiftable* if there is an integer, K, such that the shift of ψ by an arbitrary amount, $x_0 \in \mathbf{R}$, can be expressed as a linear combination of K basic shifts of ψ, i.e., if there exist *interpolation functions*, $b_k : \mathbf{R} \to \mathbf{C}$, such that

$$\psi(x - x_0) = \sum_{k=0}^{K-1} b_k(x_0)\ \psi(x - k\Delta), \tag{2.3}$$

where $\Delta = X/K$ is the basic shift amount.[4] If we let $T_{x_0} : \mathbf{R} \to \mathbf{R}$ be the translation operator defined by $T_{x_0}(x) = x - x_0$, then Eq. (2.3) is equivalent to

$$T_{x_0}\psi = \sum_{k=0}^{K-1} b_k(x_0)\ T_{k\Delta}\psi. \tag{2.4}$$

The simplest shiftable function in one dimension is a pure harmonic signal, $\psi(x) = \exp(2\pi i\omega x/X)$, for some integer ω, in which case $K = 1$. More generally, Simoncelli et al. [14] proved that any band-limited function is shiftable. Specifically, let $\hat{\psi}_k = \int_0^X \psi(x)\exp(-2\pi ikx/X)\,dx$ denote the k-th Fourier series coefficient of ψ, where $k \in \mathbf{Z}$ is an integer. If the set of non-zero Fourier series coefficients $\hat{\psi}_k$ of ψ is finite and is indexed by (a subset of) $B = \{k_0, k_0 + 1, \ldots, k_0 + K - 1\}$, then ψ can be shifted using the K interpolation functions, b_k, defined by $b_k(x_0) = b(x_0 - k\Delta)$, where

$$b(x) = \frac{1}{K}\sum_{k\in B} \exp(2\pi ikx/X) \tag{2.5}$$

is the complex conjugate of the perfect bandpass filter constructed from the set of K frequencies, B. In particular, note that the interpolation functions only depend on the set B, and not on ψ itself.

Strictly speaking, since they are neither periodic nor band-limited, functions like the Gabor, Gaussian, and derivative of Gaussian are not shiftable. However, all of these functions decay exponentially and are therefore effectively periodic. Moreover, for all intents and purposes, a function, ψ, like one of these, can be shifted by choosing the set, B, to consist of all Fourier series frequencies, k, such that the Fourier amplitude, $|\hat{\psi}_k|$, exceeds some small threshold value. Such functions will be called *effectively shiftable*.

Next recall that Freeman and Adelson [4] define a function, $\psi : \mathbf{R}^2 \to \mathbf{C}$, to be *steerable* if any arbitrary rotation of ψ about the origin in $\mathbf{R}^2$ can be expressed as a linear combination of a finite number, M, of basic rotations of ψ by amounts $m\Delta_\theta$, where $M\Delta_\theta = 2\pi$.

Now let $\Psi : \mathbf{R}^2 \times S^1 \to \mathbf{C}$ be a periodic function with period X in both spatial variables, $\vec{x}$. In analogy with the definition of a shiftable-steerable function on $\mathbf{R}^2$, we say that Ψ is *shiftable-twistable* on $\mathbf{R}^2 \times S^1$ if there are integers, K and M, and interpolation functions, $b_{\vec{k},m} : \mathbf{R}^2 \times S^1 \to \mathbf{C}$, such that, for each $(\vec{x}_0, \theta_0) \in \mathbf{R}^2 \times S^1$, the shift-twist of Ψ by $(\vec{x}_0, \theta_0)$ is a linear combination of K^2M basic shift-twists of Ψ by amounts $(\vec{k}\Delta, m\Delta_\theta)$, i.e., if

$$T_{\vec{x}_0,\theta_0}\Psi = \sum_{\vec{k},m} b_{\vec{k},m}(\vec{x}_0, \theta_0)\ T_{\vec{k}\Delta, m\Delta_\theta}\Psi. \tag{2.6}$$

Here $\Delta = X/K$ is the *basic shift amount* and $\Delta_\theta = 2\pi/M$ is the *basic twist amount*. The sum in Eq. (2.6) is taken over all pairs of integers, $\vec{k} = (k_x, k_y)$, in the range, $0 \le k_x, k_y < K$, and all integers, m, in the range, $0 \le m < M$. As we will show, for many shiftable-twistable bases, the interpolation functions, $b_{\vec{k},m}$ on $\mathbf{R}^2 \times S^1$, are defined in terms of the one-dimensional interpolation functions, b_k, defined by Eq. (2.5).

The simplest shiftable-twistable functions are those which can be twisted with $M = 1$ basic twists: $T_{\vec{0},\theta_0}\Psi = b(\theta_0)\Psi$. Such functions will be called *self-twistable*. The following Proposition shows how to construct a shiftable-twistable basis from a shiftable-twistable function.

Proposition 2.1. *Let Ψ be a shiftable-twistable function with interpolation functions, $b_{\vec{k},m}$. Then the collection of functions, $\Psi_{\vec{k},m}$, defined by*

$$\Psi_{\vec{k},m} = T_{\vec{k}\Delta, m\Delta_\theta}\Psi, \tag{2.7}$$

where Δ and Δ_θ are the basic shift and twist amounts, form a shiftable-twistable basis. More precisely, if

$$P = \sum_{\vec{\ell},n} c_{\vec{\ell},n}\ \Psi_{\vec{\ell},n}, \tag{2.8}$$

then

$$T_{\vec{x}_0,\theta_0}P = \sum_{\vec{k},m} c_{\vec{k},m}(\vec{x}_0, \theta_0)\ \Psi_{\vec{k},m}, \tag{2.9}$$

where

$$c_{\vec{k},m}(\vec{x}_0, \theta_0) = \sum_{\vec{l},n} b_{\vec{k},m}\left(R_{-n\Delta_\theta}(\vec{x}_0) + \vec{\ell}\Delta, \theta_0 + n\Delta_\theta\right) c_{\vec{\ell},n}. \tag{2.10}$$

The proof of the Proposition is a straightforward application of the following composition rule for shift-twist transformations. If $T_0 \circ T_1$ denotes the composition of two transformations defined by $(T_0 \circ T_1)(\vec{x}, \theta) = T_0(T_1(\vec{x}, \theta))$, then

$$T_{\vec{x}_0,\theta_0} \circ T_{\vec{x}_1,\theta_1} = T_{R_{-\theta_1}(\vec{x}_0)+\vec{x}_1\,,\,\theta_0+\theta_1}. \tag{2.11}$$

Details of the proof of Proposition 2.1 can be found in the Appendix.

This paper is concerned with visual computations whose input and output are functions on the continuum, $\mathbf{R}^2 \times S^1$, and which are shift-twist invariant. We propose the following general framework for performing such computations in a shift-twist invariant manner in a discrete network. First, the various states of the computation, which are functions $P : \mathbf{R}^2 \times S^1 \to \mathbf{C}$, are to be expressed in a shiftable-twistable basis, $\Psi_{\vec{k},m}$, as

$$P = \sum_{\vec{k},m} c_{\vec{k},m}\ \Psi_{\vec{k},m}, \tag{2.12}$$

where $\vec{c} = \{c_{\vec{k},m}\}$ is the *state* or *coefficient vector* of P. Second, the input state vector is to be transformed to the output state vector in a shift-twist invariant manner using a feedforward or recurrent neural network.

The biological plausibility of a given computation depends on the specific choice of shiftable-twistable basis. We conclude this section by presenting several examples of shiftable-twistable bases, in order of increasing biological plausibility and increasing complexity. In each case, the basis functions $\Psi : \mathbf{R}^2 \times S^1 \to \mathbf{C}$ are *separable*, i.e., they are the product of a periodic shiftable-steerable function, $\psi : \mathbf{R}^2 \to \mathbf{C}$ and a shiftable function, $h : S^1 \to \mathbf{C}$, i.e., $\Psi(\vec{x}, \theta) = \psi(\vec{x})h(\theta)$.

2.1. *Example A: The Gaussian-Fourier Basis*

The Gaussian-Fourier basis of functions on $\mathbf{R}^2 \times S^1$ is the product of a shiftable-steerable basis of Gaussians on $\mathbf{R}^2$ and a Fourier series basis on S^1. Let g be the radial Gaussian of standard deviation, ν, on $\mathbf{R}^2$ defined by $g(\vec{x}) = \frac{1}{\nu}\exp(-\|\vec{x}\|^2/2\nu^2)$. We regard g as a periodic function of period, X, which is chosen to be much larger than ν, so that $g(\frac{X}{2}, \frac{X}{2})$ and its derivatives are essentially zero. For each fixed frequency, $\omega \in \mathbf{Z}$, we define a function, $G_\omega : \mathbf{R}^2 \times S^1 \to \mathbf{C}$, by

$$G_\omega(\vec{x}, \theta) = g(\vec{x})\exp(i\omega\theta). \tag{2.13}$$

The following Proposition states that each of the functions, G_ω, is self-twistable. Its proof is given in the Appendix.

Proposition 2.2. *For each fixed frequency, $\omega \in \mathbf{Z}$, the periodic function, G_ω, on $\mathbf{R}^2 \times S^1$ of period X in the spatial variables, $\vec{x}$, is effectively shiftable-twistable. More precisely, let $M = 1$ and let K be the number of essentially non-zero Fourier series coefficients of the factor, $g_X(x) = \exp(-x^2/2\nu^2)$, of $g(\vec{x})$. Then, for any $(\vec{x}_0, \theta_0) \in \mathbf{R}^2 \times S^1$,*

$$T_{\vec{x}_0,\theta_0} G_\omega = \sum_{\vec{k}}\ b_{\vec{k},\omega}(\vec{x}_0, \theta_0)\ T_{\vec{k}\Delta,0} G_\omega, \tag{2.14}$$

where the interpolation functions are given by

$$b_{\vec{k},\omega}(\vec{x}_0, \theta_0) = \exp(-i\omega\theta_0)\ b_{\vec{k}}(\vec{x}_0). \tag{2.15}$$

Here $b_{\vec{k}}(\vec{x}_0) = b(\vec{x}_0 - \vec{k}\Delta)$, where

$$b(\vec{x}) = \frac{1}{K^2}\sum_{\vec{k}\in B}\exp(2\pi i\vec{k}\cdot\vec{x}/X), \tag{2.16}$$

and B is the set of K^2 indices of the essentially non-zero Fourier series coefficients of g.

By Propositions 2.1 and 2.2, for each fixed $\omega \in \mathbf{Z}$, the collection of periodic functions, $G_{\vec{k},\omega}$, defined by

$$G_{\vec{k},\omega}(\vec{x}, \theta) = (T_{\vec{k}\Delta,0} G_\omega)(\vec{x}, \theta) = g(\vec{x} - \vec{k}\Delta)\exp(i\omega\theta), \tag{2.17}$$

form an effectively shiftable-twistable basis. We define the Gaussian-Fourier basis on $\mathbf{R}^2 \times S^1$ to be the set of functions, $G_{\vec{k},\omega}$, for K^2 indices, $\vec{k} \in \mathbf{Z}^2$, parameterizing basic shifts in $\mathbf{R}^2$, and N angular frequencies, $\omega \in \mathbf{Z}$. Here N is determined by the θ-frequency content of the functions to be represented in the basis. Because G_ω is self-twistable, $\Delta_\theta = 2\pi$ and therefore Propositions 2.1 and 2.2 immediately imply the following corollary.

Corollary 2.3. *The Gaussian-Fourier basis, $G_{\vec{k},\omega}$, defined by Eq.* (2.17)*, is effectively shiftable-twistable. Consequently, if $P : \mathbf{R}^2 \times S^1 \to \mathbf{C}$ is represented in the Gaussian-Fourier basis as*

$$P = \sum_{\vec{\ell},\omega} c_{\vec{\ell},\omega} G_{\vec{\ell},\omega}, \tag{2.18}$$

then, for any $(\vec{x}_0, \theta_0) \in \mathbf{R}^2 \times S^1$, the shift-twist, $T_{\vec{x}_0,\theta_0} P$, of P can also be represented in the basis as

$$T_{\vec{x}_0,\theta_0} P = \sum_{\vec{k},\omega} c_{\vec{k},\omega}(\vec{x}_0, \theta_0)\ G_{\vec{k},\omega}, \tag{2.19}$$

where

$$c_{\vec{k},\omega}(\vec{x}_0, \theta_0) = \exp(-i\omega\theta_0) \sum_{\vec{\ell}} c_{\vec{\ell},\omega} b_{\vec{k}-\vec{\ell}}\,(\vec{x}_0). \tag{2.20}$$

In particular, Eq. (2.20) *shows that for each $\omega \in \mathbf{Z}$, the coefficient vector, $c_{\vec{k},\omega}(\vec{x}_0, \theta_0)$, of $T_{\vec{x}_0,\theta_0} P$ is obtained from the coefficient vector, $c_{\vec{k},\omega}$, of P by circular convolution with the interpolation function vector $b(\vec{x}_0)$ defined in* (2.16)*.*

Although it is not as biologically plausible as the other bases we describe, because of Eq. (2.20), a single-scale Gaussian-Fourier basis can be a very efficient basis to use in visual computations on $\mathbf{R}^2 \times S^1$, provided that the input function, P, to the computation can be represented in such a basis. For example, suppose that P is modeled as a linear combination of three-dimensional Gaussians, all of standard deviation ν in $\vec{x}$ and width η in θ, that are centered at arbitrary points, $(\vec{x}_0, \theta_0)$, in $\mathbf{R}^2 \times S^1$, i.e.,

$$P(\vec{x}, \theta) = \sum_j g(\vec{x} - \vec{x}_j) h(\theta - \theta_j), \tag{2.21}$$

where g is the Gaussian in Eq. (2.13) and where h is a Gaussian on S^1 defined by

$$h(\theta) = \frac{1}{\eta} \exp(-\theta^2/2\eta^2) = \sum_\omega \hat{h}_\omega \exp(i\omega\theta), \tag{2.22}$$

where η satisfies $\eta \ll 2\pi$, so that h can be regarded as a periodic function on S^1. Then, by Proposition 2.2, the coefficient vector, $c_{\vec{k},\omega}$, of P in the Gaussian-Fourier basis is given by

$$c_{\vec{k},\omega} = \hat{h}_\omega \sum_j b_{\vec{k}}(\vec{x}_j)\ \exp(-i\omega\theta_j). \tag{2.23}$$

2.2. *Example B: The Complex Directional Derivative of Gaussian (CDDG)–Fourier Basis*

This example is very similar to the previous one, except that the Gaussian, g on $\mathbf{R}^2$, is replaced by its complex directional derivative, ψ, in the direction of the complex valued vector, $[1, i]^{\mathrm{T}}$, defined by

$$\psi(\vec{x}) = \frac{\partial g}{\partial x} + i\frac{\partial g}{\partial y} = -\tfrac{1}{\nu^2}(x + iy) g(\vec{x}). \tag{2.24}$$

Notice that $\psi = 2\frac{\partial g}{\partial \bar{z}}$, where $z = x + iy$. Although g is not a wavelet, ψ is.[5] As in Example A, we regard ψ as a periodic function of period, X. Pictures of ψ are shown in Fig. 3. The *complex directional derivative of Gaussian (CDDG)–Fourier basis*, $\Psi_{\vec{k},\omega}$, is defined by

$$\Psi_{\vec{k},\omega}(\vec{x}, \theta) = \psi(\vec{x} - \vec{k}\Delta)\ \exp(i\omega\theta). \tag{2.25}$$

Freeman and Adelson [4] showed that the complex directional derivative of a Gaussian is self-steerable: $T_{\vec{0},\theta_0}\psi = \exp(-i\theta_0)\psi$. Similarly the function, $\Psi_\omega : \mathbf{R}^2 \times S^1 \to \mathbf{C}$ defined by $\Psi_\omega(\vec{x}, \theta) = \psi(\vec{x}) \exp(i\omega\theta)$, is self-twistable: $T_{\vec{0},\theta_0}\Psi_\omega = \exp(-i\theta_0)\exp(-i\omega\theta_0)\Psi_\omega$. As such, Ψ_ω is the simplest non-isotropic shiftable-twistable function which is localized on $\mathbf{R}^2$.

The analogies of Proposition 2.2 and Corollary 2.3 hold for the basis, $\Psi_{\vec{k},\omega}$. The only difference is that in this case, the interpolation functions in Eqs. (2.15) and (2.20) are given by

$$b_{\vec{k}}(\vec{x}_0, \theta_0) = \exp(-i\omega\theta_0)\exp(-i\theta_0)\ b_{\vec{k}}(\vec{x}_0). \tag{2.26}$$

Unlike the Gaussian-Fourier basis, the CDDG-Fourier basis has the property that its spatial factor, ψ, is a wavelet, which means that *arbitrary* input functions can be represented in a multi-scale shiftable-twistable basis constructed from the functions, Ψ_ω. We can use a *multi-scale* method to represent the input function, $P : \mathbf{R}^2 \times S^1 \to \mathbf{C}$, to a visual computation by exploiting the fact that the function, ψ on $\mathbf{R}^2$, is a mother wavelet which generates an (approximately) self-inverting, overcomplete wavelet basis [14] (i.e., an approximately tight frame [2]). Each of the wavelet basis functions, $\psi_{p,\vec{k}}$ on $\mathbf{R}^2$, is defined to be the translation by $2^{p/2}\Delta\,\vec{k}$ of the scaling of ψ by $2^{p/2}$,

$$\psi_{p,\vec{k}}(\vec{x}) = \frac{1}{2^{p/2}}\ \psi\left(\frac{\vec{x} - 2^{p/2}\Delta\vec{k}}{2^{p/2}}\right), \tag{2.27}$$

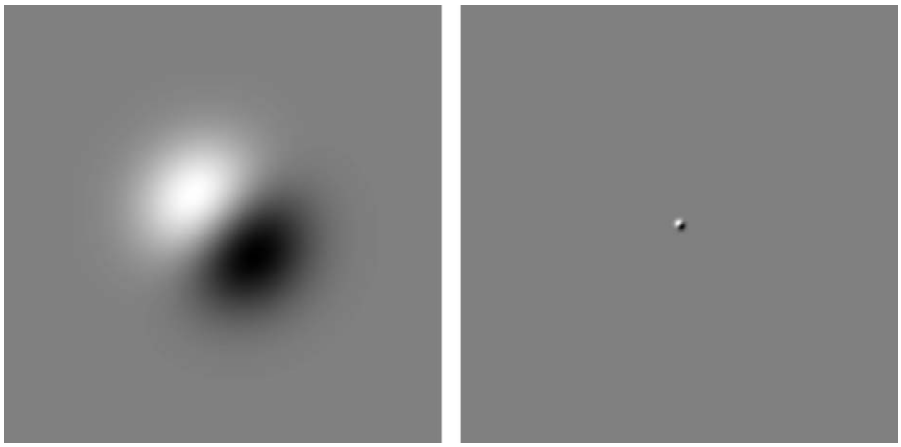

Figure 3. The real part of the complex directional derivative of a Gaussian (CDDG), steered clockwise by 45°. Left: Real part with standard deviation, $\nu = 4.0$, (with 40.0×40.0 display region). The imaginary part is the rotation of the real part, counter clockwise by 90°. Right: Real part at the finer scale, $\nu = 0.25$. The completion fields in Fig. 2 were computed by solving the Fokker-Planck equation in a CDDG-Fourier basis of this scale.

where the (scale-dependent) period, X, of the wavelet, $\psi_{p,\vec{k}}$, is chosen so that $\psi_{p,\vec{0}}(\frac{X}{2}, \frac{X}{2}) \approx 0$, and Δ is chosen so that each scale of the *wavelet-Fourier basis*, $\Psi_{p,\vec{k},\omega}$, defined by $\Psi_{p,\vec{k},\omega}(\vec{x}, \theta) = \psi_{p,\vec{k}}(\vec{x}) \exp(i\omega\theta)$, forms a shiftable-twistable basis. Even though these basis functions are neither approximately orthogonal nor linearly independent, the discussion on tight frames in [2] can be applied to show that a large class of functions, P, can be well approximated in the basis using the analysis and synthesis formulae,

$$c_{p,\vec{k},\omega} = \iiint_{\mathbf{R}^2 \times S^1} P(\vec{x}, \theta) \overline{\Psi_{p,\vec{k},\omega}(\vec{x}, \theta)}\, d\vec{x}\, d\theta, \tag{2.28}$$

where, since the functions, $\Psi_{p,\vec{k},\omega}$, form an approximately tight frame,

$$P \approx \sum_{p,\vec{k},\omega} c_{p,\vec{k},\omega}\ \Psi_{p,\vec{k},\omega}. \tag{2.29}$$

We verified numerically that by using about twelve scales, p, a Gaussian of the form (2.21) on $\mathbf{R}^2 \times S^1$ can be very well approximated using an expansion of the form (2.29). However, for simplicity, computational efficiency, and accuracy, for the visual computations in this paper we chose to represent the input function using Eq. (2.21).

2.3. *Example C: The Complex Directional Derivative of Gaussian (CDDG)—Gaussian Coupled Basis*

The complex directional derivative of a Gaussian, ψ on $\mathbf{R}^2$, is a simple edge detector. Since the real part of ψ has the preferred orientation, $\frac{\pi}{2}$, an edge centered at $\vec{x}_0$ with orientation, θ_0, will elicit a large response from the real part of $T_{\vec{x}_0,\theta_0-\frac{\pi}{2}}\psi$. Some problems in vision require that the direction or orientation of edges in an image, $I : \mathbf{R}^2 \to \mathbf{R}$, be explicitly encoded in a third variable, θ. This can be done using a coupled basis consisting of complex directional derivatives of Gaussians on $\mathbf{R}^2$ and Gaussians on S^1, where the center of the Gaussian on S^1 is coupled to the preferred orientation of the complex directional derivative of the Gaussian on $\mathbf{R}^2$.

Let h be the Gaussian on S^1 defined by Eq. (2.22), and let M be the number of essentially non-zero frequencies of h. Let ψ be the complex directional derivative of Gaussian defined in Eq. (2.24). The *complex directional derivative of Gaussian (CDDG)—Gaussian coupled basis functions*, $\Psi_{\vec{k},m}$ on $\mathbf{R}^2 \times S^1$, are defined by

$$\Psi_{\vec{k},m} = T_{\vec{k}\Delta,\, m\Delta_\theta}(\psi h). \tag{2.30}$$

Given an image, I, the function J on $\mathbf{R}^2 \times S^1$ defined by

$$J = \sum_{\vec{k},m} c_{\vec{k},m} \Psi_{\vec{k},m}, \tag{2.31}$$

explicitly encodes the position and direction of edges in I. Here,

$$c_{\vec{k},m} = \iint_{\mathbf{R}^2} I(\vec{x})\overline{\psi_{\vec{k},m}(\vec{x})}\, d\vec{x}, \tag{2.32}$$

where $\psi_{\vec{k},m} : \mathbf{R}^2 \to \mathbf{C}$ is defined by $\psi_{\vec{k},m} = T_{\vec{k}\Delta\,,\,m\Delta_\theta}\psi$.[6]

Let b_m and $b_{\vec{k}}$ denote the interpolation functions required to shift h and ψ respectively. Then the functions, $\Psi_{\vec{k},m}$, form a shiftable-twistable basis with interpolation functions[7]

$$b_{\vec{k},m}(\vec{x}_0, \theta_0) = \exp(-i\theta_0)\, \exp(im\Delta_\theta)\, b_{\vec{k}}(\vec{x}_0)\, b_m(\theta_0). \tag{2.33}$$

2.4. Example D: The Gabor-Gaussian Basis

The two-dimensional Gabor function, $\psi : \mathbf{R}^2 \to \mathbf{C}$, is defined by $\psi(x, y) = \exp(-i\xi_0(x + y))\exp(-(x^2 + y^2)/2)$, where $\exp(-(x^2 + y^2)/2)$ is a radial Gaussian and $\exp(-i\xi_0(x + y))$ is a harmonic grating of frequency, ξ_0.[8] Like the complex directional derivative of Gaussian, the Gabor possesses a preferred direction, and so one might attempt to construct a coupled Gabor-Gaussian shiftable-twistable basis. Unfortunately, such a coupled basis is not shiftable-twistable since the Gabor function cannot be written in polar coordinates, (r, ϕ), as the product of a function of r and a pure harmonic in ϕ. Stated differently, the Gabor, unlike the complex directional derivative of Gaussian, is not self-steerable. Nevertheless the uncoupled basis, $\Psi_{\vec{k},m,n}$ defined by $\Psi_{\vec{k},m,n}(\vec{x}, \theta) = (T_{\vec{k}\Delta\,,\,m\Delta_\theta}\psi)(\vec{x})\, h(\theta - n\Delta_\theta)$, is shiftable-twistable since the Gabor function, ψ on $\mathbf{R}^2$, is shiftable-steerable and the Gaussian, h, on $\mathbf{R}$ is shiftable.

3. Stochastic Completion Fields

In their computational theory of illusory contour formation, Williams and Jacobs [17] argued that, given a prior probability distribution of possible completion shapes, the visual system computes the local image plane statistics of the distribution of all possible completions, rather than simply the most probable completion. This view is in accord with human experience—some illusory contours are more salient than others, and some appear sharper than others. They defined the notion of a stochastic completion field to model illusory contours in a probabilistic manner. The stochastic completion field is a probability density function (p.d.f.) on the space, $\mathbf{R}^2 \times S^1$, of positions, $\vec{x} = (x, y)$, in the plane, $\mathbf{R}^2$, and directions, θ, in the circle, S^1. It is defined in terms of a set of position and direction constraints representing the beginning and ending points of a set of contour fragments (called *sources* and *sinks*), and a prior probability distribution of completion shapes, which is modeled as the set of paths followed by particles traveling with constant speed in directions described by Brownian motions [9]. The magnitude of the *stochastic completion field*, $C : \mathbf{R}^2 \times S^1 \to \mathbf{R}$, at a point $(\vec{x}, \theta)$, is the probability that a completion from the prior probability distribution will pass through $(\vec{x}, \theta)$ on a path joining two of the contour fragments.

The stochastic completion field is computed as follows. First, let $P(\vec{x}, \theta\,; t)$ be the probability that a particle traveling with unit speed in $\mathbf{R}^2$ in a direction described by a Brownian motion with strength, σ^2, on S^1 is at the point, $(\vec{x}, \theta)$, at time, t, given that it decays with a half-life, τ, and that it was sampled from an initial probability distribution of sources, $P(\vec{x}, \theta\,; 0)$, at time, $t = 0$. Mumford observed that P evolves according to a Fokker-Planck equation of the form,

$$\frac{\partial P}{\partial t} = -\cos\theta \frac{\partial P}{\partial x} - \sin\theta \frac{\partial P}{\partial y} + \frac{\sigma^2}{2}\frac{\partial^2 P}{\partial \theta^2} - \frac{1}{\tau}P, \tag{3.1}$$

where the initial probability distribution of sources (or sinks) is described by $P(\vec{x}, \theta\,; 0)$. This partial differential equation can be viewed as a set of independent *advection* equations in $\vec{x} = (x, y)$ (the first and second terms) coupled in the θ dimension by the *diffusion* equation (the third term). The advection equations translate probability mass in direction θ with unit speed, while the diffusion term models the Brownian motion in direction, with *diffusion parameter*, σ. The combined effect of these three terms is that particles tend to travel in straight lines, but over time they drift to the left or right by an amount proportional to σ^2. Finally, the effect of the fourth term is that particles decay over time, with a half life given by the *decay constant*, τ. This represents our prior expectation on the length of gaps—most are quite short.

Williams and Jacobs [17] showed that the stochastic completion field could be factored into a *source field*, $P' : \mathbf{R}^2 \times S^1 \to \mathbf{R}$, and a *sink field*, $Q' : \mathbf{R}^2 \times S^1 \to \mathbf{R}$. The value of the source field, P' at $(\vec{x}, \theta)$, represents the probability that a contour beginning at a source will

pass through $(\vec{x}, \theta)$. It is defined by

$$P'(\vec{x}, \theta) = \int_0^\infty P(\vec{x}, \theta\,; t)\, dt, \tag{3.2}$$

where the initial p.d.f., $P(\vec{x}, \theta\,; 0)$, represents the initial distribution of sources. The value of the sink field, Q' at $(\vec{x}, \theta)$, represents the probability that a contour beginning at $(\vec{x}, \theta)$ will reach a sink. Since the probability that a contour joins $(\vec{x}, \theta)$ to $(\vec{u}, \phi)$ is equal to the probability that a contour joins $(\vec{u}, \phi + \pi)$ to $(\vec{x}, \theta + \pi)$, the sink field can be defined as follows. Let $Q(\vec{x}, \theta\,; 0)$ represent the initial distribution of sinks, and let $\tilde{Q}(\vec{x}, \theta\,; t)$ be the solution of the Fokker-Planck equation with initial condition, $\tilde{Q}(\vec{x}, \theta\,; 0) = Q(\vec{x}, \theta + \pi\,; 0)$. Then the sink field, Q', is defined by

$$Q'(\vec{x}, \theta) = \int_0^\infty Q(\vec{x}, \theta\,; t)\, dt, \tag{3.3}$$

where $Q(\vec{x}, \theta\,; t) = \tilde{Q}(\vec{x}, \theta + \pi\,; t)$. Finally, the completion field is given by

$$C = P' \cdot\ Q'. \tag{3.4}$$

In Williams and Jacobs [18] stochastic completion fields were computed by solving the Fokker-Planck equation using a standard finite differencing scheme on a regular grid.

In Williams and Jacobs [17, 18] the initial sources and sinks were extracted automatically from the input image using steerable filters [13] to identify corners and measure orientations. However, this method should only be regarded as an interim solution to the problem of specifying initial conditions given a brightness image, since we believe that in the long term, the solution lies in the generalization of the notion of a completion field described in [19]. For this reason and for convenience's sake, in all experiments in this paper, the initial sources and sinks were specified by hand.

4. Description of Algorithm

One of the main goals of this paper is to derive a discrete numerical algorithm to compute stochastic completion fields in a shift-twist invariant manner. This invariance is achieved by first evolving the Fokker-Planck equation in a shiftable-twistable basis of $\mathbf{R}^2 \times S^1$ to obtain representations of the source and sink fields in the basis, and then multiplying these representations in a shift-twist invariant manner to obtain a representation of the completion field in a shiftable-twistable basis. We observe that a discrete Dirac basis, consisting of functions,

$$\delta_{\vec{k},m} = T_{\vec{k}\Delta\,, m\Delta_\theta}\delta, \tag{4.1}$$

where δ is the Dirac delta function at $(\vec{0}, 0)$, and where $(\vec{k}, m)$ is a triple of integers, is not shiftable-twistable. This is because a Dirac function located off the grid of Dirac basis functions is not in their span. A major shortcoming of all previous contour completion algorithms [5, 6, 8, 10, 12, 17, 18, 22] is that they perform computations in this basis. As a consequence, initial conditions which do not lie directly on the grid cannot be accurately represented. This problem is often skirted by researchers in this area by choosing input patterns which match their choice of sampling rate and phase. For example, Li [8] used only six orientations (including 0°) and Heitger and von der Heydt [6], only twelve (including 0°, 60° and 120°). Li's first test pattern was a line of orientation, 0°, while Heitger and von der Heydt used a Kanizsa Triangle with sides of 0°, 60°, and 120° orientation. There is no reason to believe that the experimental results they show would be the same if their input patterns were rotated by as little as 5°.[9]

In addition to the problem of representing the input, the computation itself must be Euclidean invariant. Stochastic completion fields computed using the finite differencing scheme of [18] exhibit marked anisotropic spatial smoothing due to the manner in which advection on $\mathbf{R}^2$ is performed on a grid (see Figs. 8–10). Although probability mass advects perfectly in either of the two principal coordinate directions, mass which is moving at an angle to the grid gradually disperses, since, at each time step, bilinear interpolation is used to place the mass on the grid. One way to restore the isotropy of the advection transformation is to carefully add extra spatial smoothing [21].

Stochastic completion fields can be computed using any of the shiftable-twistable bases in Section 2. For reasons of simplicity, in this paper, we chose to perform the computation in a Gaussian-Fourier basis. Using Eq. (2.21), we model the initial distribution of edge fragments using three-dimensional Gaussians of a fixed fine scale whose centers are determined by the locations and directions of the edge fragments. The initial distribution, $P(\vec{x}, \theta\,; 0)$, is represented in a Gaussian-Fourier basis, $G_{\vec{k},\omega}$, using Eq. (2.18) with an initial coefficient vector, $c(0) = \{c_{\vec{k},\omega}(0)\}$, given by Eq. (2.23).

To solve the Fokker-Planck equation, we express its solution, $P(\vec{x}, \theta\,; t)$, in terms of the basis functions, $G_{\vec{k},\omega}$, as

$$P(\vec{x}, \theta\,; t) = \sum_{\vec{k},\omega} c_{\vec{k},\omega}(t)\, G_{\vec{k},\omega}(\vec{x}, \theta), \tag{4.2}$$

where the coefficient vector, $c(t) = \{c_{\vec{k},\omega}(t)\}$, depends on time. As is explained in Section 5, we derive a linear transformation, $c(t + \Delta t) = (\mathbf{A} \circ \mathbf{D})c(t)$, to evolve the coefficient vector in time. This transformation is the composition of an advection transformation, $\mathbf{A}$, which has the effect of transporting probability mass in directions θ, and a diffusion-decay transformation, $\mathbf{D}$, which implements both the diffusion of mass in θ, and the decay of mass over time.

If we represent the source field P' in the Gaussian-Fourier basis as

$$P' = \sum_{\vec{k},\omega} p'_{\vec{k},\omega}\, G_{\vec{k},\omega}, \tag{4.3}$$

then the source field coefficient vector, $p' = \{p'_{\vec{k},\omega}\}$, is given by

$$p'_{\vec{k},\omega} = \int_0^\infty p_{\vec{k},\omega}(t)\, dt, \tag{4.4}$$

where $p_{\vec{k},\omega}(t)$ is the coefficient vector of the solution of the Fokker-Planck equation in the basis at time t, and where the initial coefficient vector, $p(0)$, is determined by the sources, using Eq. (2.23). Similarly, we represent the sink field, Q', in the basis as

$$Q' = \sum_{\vec{k},\omega} q'_{\vec{k},\omega}\, G_{\vec{k},\omega}, \tag{4.5}$$

where the sink field coefficient vector, $q' = \{q'_{\vec{k},\omega}\}$, is defined analogously to p'.

The shiftability-twistability of the basis functions is used in two distinct ways to obtain shift-twist invariant source and sink fields. First, it enables any two initial conditions, which are related by an arbitrary transformation, $T_{\vec{x}_0,\theta_0}$, to be represented equally well in the basis. Second, it is used to derive a shift-twist invariant advection transformation, $\mathbf{A}$, thereby eliminating the grid orientation artifacts described above. In summary, given a desired resolution at which to represent the initial conditions, our new algorithm produces source and sink fields, at the given resolution, which transform appropriately under arbitrary Euclidean transformations of the input image. In contrast, in all previous contour completion algorithms, the degree of failure of Euclidean invariance is highly dependent on the resolution of the grid, and can be quite large relative to the grid resolution.

The final step in our shift-twist invariant algorithm is to compute the completion field (which by Eq. (3.4) is the product of the source and sink fields) in a shiftable-twistable basis. As we explain in Section 6, the particular basis used to represent the completion field is the same as the one used to represent the source and sink fields, except that the variance of the Gaussian basis functions in $\mathbf{R}^2$ needs to be halved.[10]

5. The Solution of the Fokker-Planck Equation

In this section we derive a shift-twist invariant linear transformation,

$$c(t + \Delta t) = (\mathbf{A} \circ \mathbf{D})c(t), \tag{5.1}$$

of the coefficient vector, $c(t) = \{c_{\vec{k},\omega}(t)\}$, which evolves the Fokker-Planck equation in a shiftable-twistable basis. The action, $c(t + \Delta t) = \mathbf{D}c(t)$, of the diffusion operator on the coefficient vector corresponds to solving

$$\frac{\partial P}{\partial t} = \frac{\sigma^2}{2}\frac{\partial^2 P}{\partial \theta^2} \; - \; \frac{1}{\tau} P, \tag{5.2}$$

and the action, $c(t + \Delta t) = \mathbf{A}c(t)$, of the advection operator corresponds to solving

$$\frac{\partial P}{\partial t} = -\cos\theta \frac{\partial P}{\partial x} \; - \; \sin\theta \frac{\partial P}{\partial y}, \tag{5.3}$$

both from t to $t + \Delta t$. We numerically compute a solution to the Fokker-Planck equation at time, t, by alternately applying the diffusion and advection operators to c, using many small time steps of size, Δt.

Our derivation holds for any shiftable-twistable basis constructed from shiftable-twistable functions of the form, $\Psi_\omega(\vec{x}, \theta) = \psi(\vec{x}) \exp(i\omega\theta)$, for some function, ψ on $\mathbf{R}^2$. Since the transformation, $\mathbf{A} \circ \mathbf{D}$, will only involve interactions between functions, ψ, at different positions $\vec{k}\Delta$, and not at different orientations or scales, the basis functions and coefficients will be denoted by $\Psi_{\vec{k},\omega} = T_{\vec{k}\Delta,0}\Psi_\omega$ and $c_{\vec{k},\omega}(t)$ respectively.

To derive an expression,

$$c_{\vec{\ell},\eta}(t + \Delta t) = \sum_{\vec{k},\omega} \mathbf{A}_{\vec{\ell},\eta\,;\vec{k},\omega}(\Delta t)\; c_{\vec{k},\omega}(t), \tag{5.4}$$

for the advection transformation, $\mathbf{A}$, in the basis, $\Psi_{\vec{k},\omega}$, we exploit the fact that advection on $\mathbf{R}^2$ in a direction θ can be done perfectly using shiftable basis functions, $\psi_{\vec{k}} = T_{\vec{k}\Delta,0}\psi$, on $\mathbf{R}^2$, and the continuous variable, $\theta \in S^1$. Suppose that P is given in the form,

$$P(\vec{x},\theta;\,t) = \sum_{\vec{k},\omega} c_{\vec{k},\omega}(t)\,\psi_{\vec{k}}(\vec{x})\exp(i\omega\theta) = \sum_{\vec{k}} \check{c}_{\vec{k},\theta}(t)\,\psi_{\vec{k}}(\vec{x}), \tag{5.5}$$

where $\check{c}(t)$ is related to $c(t)$ by the standard synthesis formula for Fourier series on S^1, $\check{c}_{\vec{k},\theta} = \sum_\omega c_{\vec{k},\omega}\exp(i\omega\theta)$, which we denote by $\check{c} = \mathbf{F}^{-1}c$. Since translation in $\mathbf{R}^2$ in direction θ at unit speed for time Δt is a translation by $\vec{x}_0 = \Delta t[\cos\theta, \sin\theta]^{\mathrm{T}}$, we have that

$$\begin{aligned} &P(\vec{x},\theta;t+\Delta t)\\ &\quad= P(\vec{x}-\Delta t[\cos\theta,\sin\theta]^{\mathrm{T}},\theta\,;t) &(5.6)\\ &\quad= \sum_{\vec{k}} \check{c}_{\vec{k},\theta}(t)\psi_{\vec{k}}(\vec{x}-\Delta t[\cos\theta,\sin\theta]^{\mathrm{T}}), &(5.7)\end{aligned}$$

where the second equation follows from Eq. (5.5). The shiftability of ψ then implies that

$$\check{c}_{\vec{\ell},\theta}(t+\Delta t) = \sum_{\vec{k}} \check{\mathbf{A}}_{\vec{\ell},\theta;\vec{k},\theta}(\Delta t)\;\check{c}_{\vec{k},\theta}(t), \tag{5.8}$$

where

$$\check{\mathbf{A}}_{\vec{\ell},\theta;\vec{k},\theta}(\Delta t) = b_{\vec{\ell}-\vec{k}}(\Delta t[\cos\theta,\sin\theta]^{\mathrm{T}}), \tag{5.9}$$

and $b_{\vec{k}}$ is defined in (2.16).

Finally, the advection transformation, $\mathbf{A}$, in the basis, $\Psi_{\vec{k},\omega}$, is given by the similarity transformation, $\mathbf{A} = \mathbf{F}\check{\mathbf{A}}\mathbf{F}^{-1}$, where $\mathbf{F}$ denotes the standard analysis formula for Fourier series, $(\mathbf{F}f)(\omega) = \frac{1}{2\pi}\int_0^{2\pi} f(\theta)\exp(-i\omega\theta)\,d\theta$. Since $c = \mathbf{F}\check{c}$ we have the following result.

Theorem 5.1. *In the shiftable-twistable basis, $\Psi_{\vec{k},\omega}$, the advection transformation, $\mathbf{A}$, is given by*

$$c_{\vec{\ell},\eta}(t+\Delta t) = \sum_{\vec{k},\omega} \hat{b}_{\vec{\ell}-\vec{k},\eta-\omega}(\Delta t)\;c_{\vec{k},\omega}(t), \tag{5.10}$$

where

$$\hat{b}_{\vec{k},\eta}(\Delta t) = \frac{1}{2\pi}\int_0^{2\pi} b_{\vec{k}}(\Delta t[\cos\theta,\sin\theta]^{\mathrm{T}})\exp(-i\eta\theta)\,d\theta. \tag{5.11}$$

In particular, the transformation, $\mathbf{A}$, is shift-twist invariant and is a convolution operator on the vector space of coefficients, $c_{\vec{k},\omega}$.

The proof of the shift-twist invariance of $\mathbf{A}$ is given in the Appendix.

The degree of accuracy with which the discrete advection transformation, $\mathbf{A}$, models the continuous advection process is determined by the number of basis functions in the shiftable-twistable basis. In order to prevent aliasing in the representation of P in the basis, the set of Fourier series frequencies, ω, must be large enough to capture the θ-frequency content of the p.d.f., $P(\vec{x},\theta;\,t)$. Suppose that the initial p.d.f. is the Gaussian-Fourier basis function, $P(\vec{x},\theta;\,0) = G_\omega(\vec{x},\theta) = g(\vec{x})\exp(i\omega\theta)$. Then the advection, $P(\vec{x},\theta;\,t) = P(\vec{x}-t[\cos\theta,\sin\theta]^{\mathrm{T}},\theta;\,0)$, of P can be described as follows. For each fixed angle, θ, the function, g is translated in $\mathbf{R}^2$ by t units in the direction, θ, and weighted by the factor, $\exp(i\omega\theta)$. Consequently, at time, t, the p.d.f. is supported on a neighborhood of a helix[11] of radius, t, oriented about the θ-axis in $\mathbf{R}^2\times S^1$.

Consider the case that the initial p.d.f., $P(\vec{x},\theta;\,0)$, is the Gaussian-Fourier basis function, $P(\vec{x},\theta;\,0) = G_{\vec{0},12}(\vec{x},\theta) = \exp(-8.0\|\vec{x}\|^2)\exp(12i\theta)$ (of period $X = 40.0$), where the basis consists of $K = 160$ basic shifts in the x and y variables and 176 frequencies, ω, in the θ variable. Figure 4 (left) shows the integral over S^1 of the advection of $P(\vec{x},\theta;\,0)$ at time, $t = 14.0$, i.e., $\int_0^{2\pi} P(\vec{x},\theta;\,14.0)\,d\theta$. In particular, note that $\int_0^{2\pi} P(\vec{x},\theta;\,14.0)\,d\theta$ is supported on a circle of radius 14.0, which is the projection from $\mathbf{R}^2\times S^1$ to $\mathbf{R}^2$ of the helical support of $P(\vec{x},\theta;\,14.0)$.

Coupling the θ-diffusion process to the advection process decreases the θ-frequency content of the p.d.f., $P(\vec{x},\theta;\,t)$, and so fewer Fourier series frequencies are required in the basis. For example, if the diffusion parameter is $\sigma = 0.08$, then the number of θ-frequencies can be reduced from 176 to 92. Figure 4 (right) shows the integral over S^1 of the source field obtained by evolving the initial p.d.f., $G_{\vec{0},12}$, according to

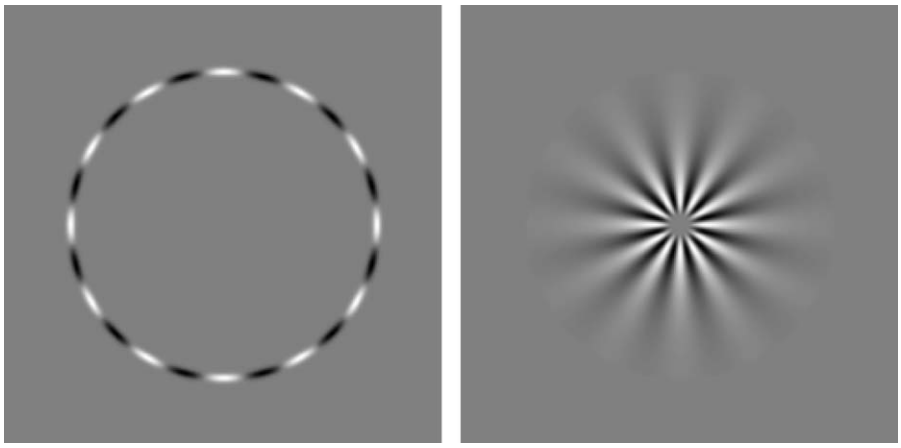

Figure 4. Left: The integral over S^1 of the advection of the Gaussian-Fourier basis function, $G_{\vec{0},12}$ on $\mathbf{R}^2 \times S^1$, at time $t = 14.0$. Right: The integral over S^1 of the source field, $P'(\vec{x}, \theta) \approx \int_0^{14.0} P(\vec{x}, \theta; t)dt$, where $P(\vec{x}, \theta; t)$ is the solution of the Fokker-Planck equation, with initial conditions given by the basis function, $G_{\vec{0},12}$.

the Fokker-Planck equation, with diffusion parameter, $\sigma = 0.08$ and decay constant, $\tau = 15.0$.

The θ-frequency content of the helical p.d.f. and the accuracy of the advection process are analyzed in the Appendix. This analysis implies that if the spatial resolution of the Gaussian initial conditions is increased by a factor of two in all three variables, $(\vec{x}, \theta)$, then the number of basis functions must be multiplied by sixteen to ensure the same degree of accuracy in the advection of the initial conditions.[12]

The diffusion-decay transformation, $c(t + \Delta t) = \mathbf{D}c(t)$, which we use, is given in the following Proposition, the proof of which is in the Appendix.

Proposition 5.2. *Let N be the number of Fourier series frequencies, ω, used in the shiftable-twistable basis, and let $\Delta\theta = 2\pi/N$. The diffusion-decay transformation, $\mathbf{D}$, is given by*

$$c_{\vec{k},\omega}(t + \Delta t) = \exp(-\Delta t/\tau)\,[\lambda \exp(-i\omega\Delta\theta) + (1 - 2\lambda) + \lambda \exp(i\omega\Delta\theta)]\, c_{\vec{k},\omega}(t), \tag{5.12}$$

where $\lambda = \frac{\sigma^2}{2}\frac{\Delta t}{(\Delta\theta)^2}$. Furthermore, $\mathbf{D}$ is shift-twist invariant.[13]

The factor, $\lambda \exp(-i\omega\Delta\theta) + (1 - 2\lambda) + \lambda \exp(i\omega\Delta\theta)$, in Eq. (5.12) is the transfer function for the diffusion equation, and the factor, $\exp(-\Delta t/\tau)$, implements the decay. If $c_{\vec{k},\omega}(t)$ evolves according to Eq. (5.12), then $P(\vec{x}, \theta\,; t)$ evolves according to the standard, explicit, 3-point stencil finite differencing scheme for diffusion in θ and exponential decay in time. In particular, if Δt is chosen so that $\lambda \leq 0.5$, then this finite differencing scheme is stable.

Theorem 5.1 and Proposition 5.2 imply that the computation of source and sink fields can be performed in a recurrent neural network using a fixed set of units as described in [18]. Furthermore, the resulting source and sink field coefficient vectors only depend on the initial data and on the set of (essentially) non-zero Fourier series frequencies of the basis function, ψ.

Since the advection transformation, $\mathbf{A}$, is a convolution operator on the space of coefficients, for efficiency's sake we implemented both $\mathbf{A}$ and $\mathbf{D}$ in the 3D Fourier domain of the coefficient vector. In this domain, $\mathbf{A}$ is given by a diagonal matrix and $\mathbf{D}$ by a circulant tridiagonal matrix.

6. Completion Fields in the Basis

The representation of completion fields in the Gaussian-Fourier basis uses basis functions on $\mathbf{R}^2$ which have half the variance of those used to represent source and sink fields. The reason we need to use finer scale basis functions is that the product of the Gaussian, $\exp(-x^2/2)$, with itself is the finer scale Gaussian, $\exp(-x^2)$. The superscript " $\widetilde{\ }$ " will be used to refer to the finer scale basis. Set $\widetilde{\nu} = \nu/\sqrt{2}$, $\widetilde{\Delta} = \Delta/\sqrt{2}$, $\widetilde{K} = \sqrt{2}K$ and $\widetilde{N} = N$, and define

$\widetilde{g}(\vec{x}) = g(\sqrt{2}\vec{x}) = \exp(-\|\vec{x}\|^2/2\widetilde{\nu}^2)$. Then the corresponding Gaussian-Fourier basis, $\widetilde{G}_{\vec{j},\underline{\alpha}}$, is shiftable-twistable, with interpolation functions, $\widetilde{b}_{\vec{j}}$.

Recall from Eq. (3.4) that the completion field, C on $\mathbf{R}^2 \times S^1$, is the product of the source and sink fields, $C = P' \cdot Q'$, where we represent the source and sink fields in the Gaussian-Fourier basis $G_{\vec{k},\omega}$ as in Eqs. (4.3) and (4.5), respectively. To represent the completion field in the Gaussian-Fourier basis, $\widetilde{G}_{\vec{j},\alpha}$, it suffices to express the product, $G_{\vec{k},\omega}G_{\vec{\ell},\eta}$, of two basis functions in the basis, $\widetilde{G}_{\vec{j},\alpha}$. In the Appendix we prove the product formula[14]

$$G_{\vec{k},\omega}G_{\vec{\ell},\eta} = \frac{1}{2\widetilde{\nu}} \exp\left[-\left(\frac{\widetilde{\Delta}}{2\widetilde{\nu}}\|\vec{k}-\vec{\ell}\|\right)^2\right] \times \sum_{\vec{j}} \widetilde{b}_{\vec{j}}\left[\frac{\widetilde{\Delta}}{\sqrt{2}}(\vec{k}+\vec{\ell})\right]\widetilde{G}_{\vec{j},\omega+\eta}. \quad (6.1)$$

Combining this product formula with Eqs. (4.3) and (4.5) gives the following Theorem.

Theorem 6.1. *The expression for the completion field, C on $\mathbf{R}^2 \times S^1$, in the Gaussian-Fourier basis $\widetilde{G}_{\vec{j},\alpha}$ is given by*

$$C = \sum_{\vec{j},\alpha} C_{\vec{j},\alpha}\, \widetilde{G}_{\vec{j},\alpha}, \quad (6.2)$$

where the completion field coefficient vector, $C_{\vec{j},\alpha}$, is given by

$$C_{\vec{j},\alpha} = \frac{1}{2\widetilde{\nu}} \sum_{\vec{k},\vec{\ell}} \sum_{\beta} p'_{\vec{k},\beta}\, q'_{\vec{\ell},\alpha-\beta} \times \exp\left[-\left(\frac{\widetilde{\Delta}}{2\widetilde{\nu}}\|\vec{k}-\vec{\ell}\|\right)^2\right] \times \sum_{\vec{j}} \widetilde{b}_{\vec{j}}\left[\frac{\widetilde{\Delta}}{\sqrt{2}}(\vec{k}+\vec{\ell})\right], \quad (6.3)$$

where $p'_{\vec{k},\omega}$ and $q'_{\vec{\ell},\eta}$ are the source and sink field coefficient vectors.

In particular, the calculation of $C_{\vec{j},\alpha}$ from the initial source and sink coefficient vectors, $p_{\vec{k},\omega}(0)$ and $q_{\vec{\ell},\eta}(0)$, can be performed in a recurrent neural network using a fixed set of units as described in [18].

It is helpful to observe two features of Eq. (6.3). First, the presence of the Gaussian factor involving $\|\vec{k}-\vec{\ell}\|$ means that in practice, the sum can be taken only over those indices $\vec{k}$ and $\vec{\ell}$ for which $\|\vec{k}-\vec{\ell}\|$ is quite small, i.e., only spatially proximal pairs of source and sink field coefficients need to interact to compute the completion field coefficient vector. Second, the circular convolution of $p'_{\vec{k},\alpha}$ and $q'_{\vec{\ell},\beta}$ in the frequency variable, α, corresponds to multiplication in the θ variable, which occurs when the completion field is constructed from the source and sink fields.

7. Completion Fields in the CDDG—Fourier Basis

The algorithm we have presented for computing stochastic completion fields in the Gaussian-Fourier basis can be interpreted as a computation in the more biologically plausible complex directional derivative of Gaussian (CDDG)-Fourier basis. As in the Gaussian-Fourier basis, a single scale basis of functions, $\Psi_{\vec{k},\omega}$ on $\mathbf{R}^2 \times S^1$ defined by Eq. (2.25), is used to represent the initial conditions and solve the Fokker-Planck equation.

Rather than solving the Fokker-Planck equation with Gaussian initial conditions, as in Eq. (2.24), we take a directional derivative in the spatial variables, $\vec{x}$, of the initial conditions (2.21) to obtain new initial conditions which can be represented in the CDDG-Fourier basis using the coefficient vector given by (2.23). Using the directional derivatives of the initial sources as initial conditions, a *source field coefficient vector*, $p'_{\vec{k},\omega}$, is obtained by solving the Fokker-Planck equation in the basis. In this manner we obtain a representation of a derivative of the source field in the CDDG-Fourier basis:

$$\mathbb{D}(P') = \sum_{\vec{k},\omega} p'_{\vec{k},\omega}\, \Psi_{\vec{k},\omega}, \quad (7.1)$$

where $\mathbb{D}$ is the operator, $\mathbb{D} = \frac{\partial}{\partial x} + i\frac{\partial}{\partial y}$, in Eq. (2.24). A representation of the source field itself can be obtained by integrating Eq. (7.1) as follows. Let $G_{\vec{k},\omega}$ be the Gaussian-Fourier basis function defined in Eq. (2.17). By Eq. (2.24), $\Psi_{\vec{k},\omega} = \mathbb{D}G_{\vec{k},\omega}$. Therefore, by Eq. (7.1), the source field can be represented in the Gaussian-Fourier basis as [15]

$$P' = \sum_{\vec{k},\omega} p'_{\vec{k},\omega}\, G_{\vec{k},\omega}. \quad (7.2)$$

Note that the two source field coefficient vectors, $p'_{\vec{k},\omega}$, obtained by solving the Fokker-Planck equation in the

two bases, $\Psi_{\vec{k},\omega}$ and $G_{\vec{k},\omega}$ are *identical*, since the frequency content of G_ω and Ψ_ω are essentially the same and since the source field coefficient vector, $p'_{\vec{k},\omega}$, only depends on the interpolation functions, $b_{\vec{k}}$, and on the locations and directions of the source initial conditions. Finally, the expression for the directional derivative, $\mathbb{D}C$, of the completion field in the CDDG-Fourier basis is given by

$$\mathbb{D}C = \sum_{\vec{j},\alpha} C_{\vec{j},\alpha}\, \widetilde{\Psi}_{\vec{j},\alpha}, \tag{7.3}$$

where $C_{\vec{j},\alpha}$ is given by Eq. (6.3).

8. Experimental Results

We present four experiments demonstrating the Euclidean invariance of our algorithm. In each experiment, the Gaussian-Fourier basis consisted of $K = 160$ translates in each spatial variable of a Gaussian (of period $X = 40.0$ units), and harmonic signals of $N = 92$ frequencies in the angular variable, for a total of 2.355×10^6 basis functions. Pictures of completion fields were obtained by analytically integrating over S^1 and rendering the completion field on a 256×256 grid.

In the first experiment, we computed source fields using the new algorithm. The diffusion parameter was $\sigma = 0.12$, the decay constant, $\tau = 25.0$, and the time increment, $\Delta t = 0.1$. The left column of Fig. 5 shows the p.d.f. and source field due to a single three-dimensional Gaussian initial condition centered at $(\vec{x}_0, \theta_0) = (-16.0, 0.0, 0^\circ)$, while in the right column the initial condition has been shifted and twisted to be centered at $(\vec{x}_0, \theta_0) = (-14.125, -12.875, 45^\circ)$. The p.d.f.'s are shown at time, $t = 30.0$, and the source fields were obtained by integrating the p.d.f. up to time, $t = 30.0$. The source fields were clipped above at 5×10^{-4}.

In the remaining experiments, we compare the new algorithm with the finite differencing scheme of [18]. For the finite differencing scheme, the $40.0 \times 40.0 \times 2\pi$ space was discretized using a 256×256 spatial grid with 36 discrete orientations, for a total of 2.359×10^6 Dirac basis functions. The intent was to use approximately the same number of basis functions for both algorithms. The initial conditions were represented on the grid using tri-linear interpolation and pictures of the completion fields were obtained by summing over the discrete angles. The same parameters were used for both algorithms. The decay constant was $\tau = 4.5$ and the time increment, $\Delta t = 0.1$. The diffusion parameter was $\sigma = 0.08$ for the second and third experiments and $\sigma = 0.14$ for the last.[16] In Figs. 8–10 the completion fields constructed using the algorithm of [18] are in the left column, while those constructed using the new algorithm are in the right column.

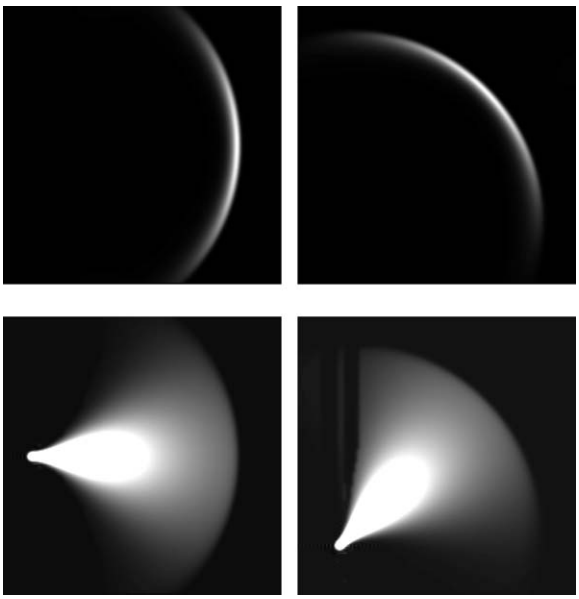

Figure 5. Probability density functions and source fields due to a single 3D Gaussian initial condition centered at a point, $(\vec{x}_0, \theta_0)$, computed using the new algorithm. The p.d.f.'s are shown at time, $t = 30.0$, and the source fields are integrated out to time, $t = 30.0$. Top left: P.d.f., $P(\vec{x}, \theta; 30.0)$, with initial condition centered at $(\vec{x}_0, \theta_0) = (-16.0, 0.0, 0^\circ)$. Top right: P.d.f. with $(\vec{x}_0, \theta_0) = (-14.125, -12.875, 45^\circ)$. Bottom left: Source field, $P'(\vec{x}, \theta) \approx \int_0^{30.0} P(\vec{x}, \theta; t)\, dt$, with $(\vec{x}_0, \theta_0) = (-16.0, 0.0, 0^\circ)$. Bottom right: Source field with $(\vec{x}_0, \theta_0) = (-14.125, -12.875, 45^\circ)$.

In the second experiment, we computed straight line completion fields joining two diametrically opposed points on a circle of radius, 16.0, with initial directions normal to the circle. That is, given an angle, ϕ, the initial stimulus consisted of the two points, $(\pm 16.0 \cos\phi, \pm 16.0 \sin\phi, \phi)$, see Fig. 6 (left). The completion fields are shown in Fig. 8, with those in the left column, computed using the method of [18], clipped above at 2×10^{-6}.

To evaluate the Euclidean invariance of the new algorithm, we extracted a section of each completion field along the diameter of the circle normal to the direction of the completion field (see Fig. 6). In Fig. 7, we plot the mean of each section as a function of the angle, ϕ. The dashed line indicates the means computed

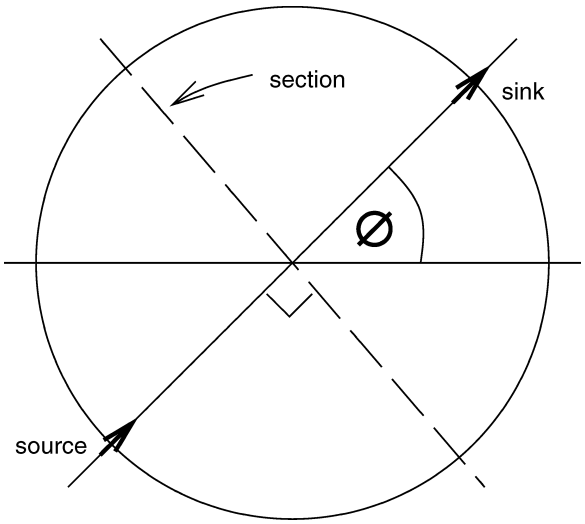

Figure 6. The geometry of the straight line completion field experiment.

using the new algorithm, and the solid line shows the means computed using the first-order, explicit Euler method described by Williams and Jacobs [18].[17] The fact that the dashed line graph is constant provides solid evidence for the Euclidean invariance of the new algorithm. The solid line graph demonstrates the two major sources of the lack of Euclidean invariance in the method of described by Williams and Jacobs [18]. First, the rapid oscillation of period 10° is due to the initial conditions coming in and out of phase with the angular grid. This 10° periodicity can be seen in the periodicity of the general shape of the completion fields in the left column of Fig. 8. Second, the large spikes at 90° intervals are due to the anisotropic manner in which the advection transformation was solved on the spatial grid. These large spikes correspond to the very bright horizontal line artifacts in the first two completion fields in the left column of Fig. 8.

In the third experiment, we computed completion fields due to rotations of the Ehrenstein initial stimulus in Fig. 1(a). Pictures of the completion fields are shown in Fig. 9.[18] The top row shows the completion fields due to the Ehrenstein stimulus in Fig. 1(a), while in subsequent rows, the initial conditions have been rotated clockwise through angles, $\theta_0 = 5°$, 15°, and 45°. The completion fields computed using the method of Williams and Jacobs [18] were clipped above at 1.25×10^{-8}. For our final experiment, we compute

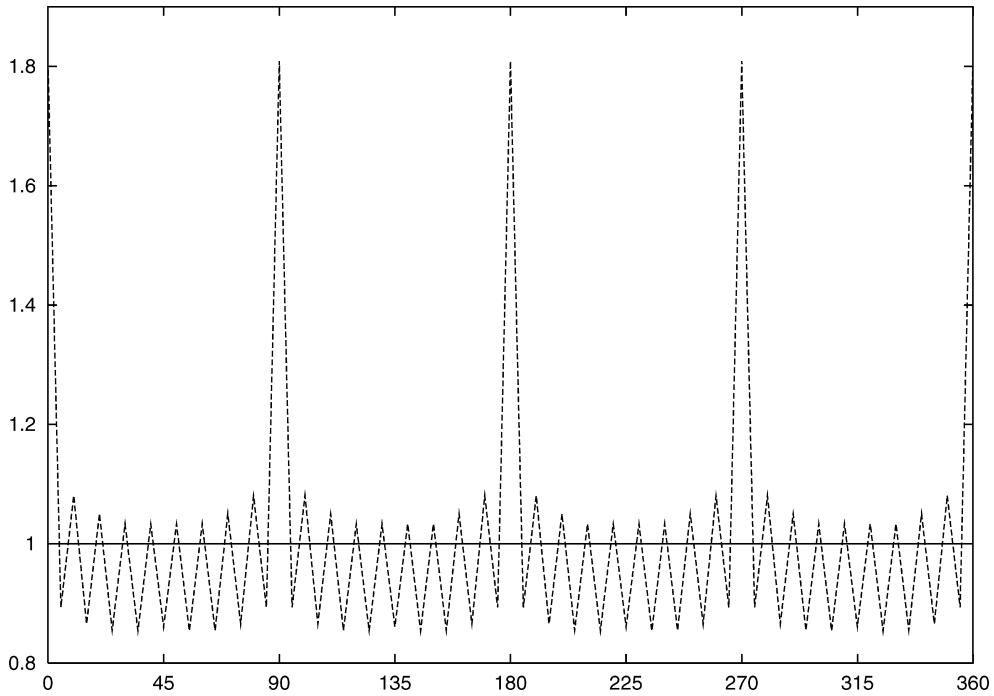

Figure 7. Graph of the mean along a section normal to the straight line completion field as a function of the direction, ϕ. Solid line: Using shiftable-twistable functions. Dashed line: Using the first-order, explicit, Euler method described in Williams and Jacobs [18].

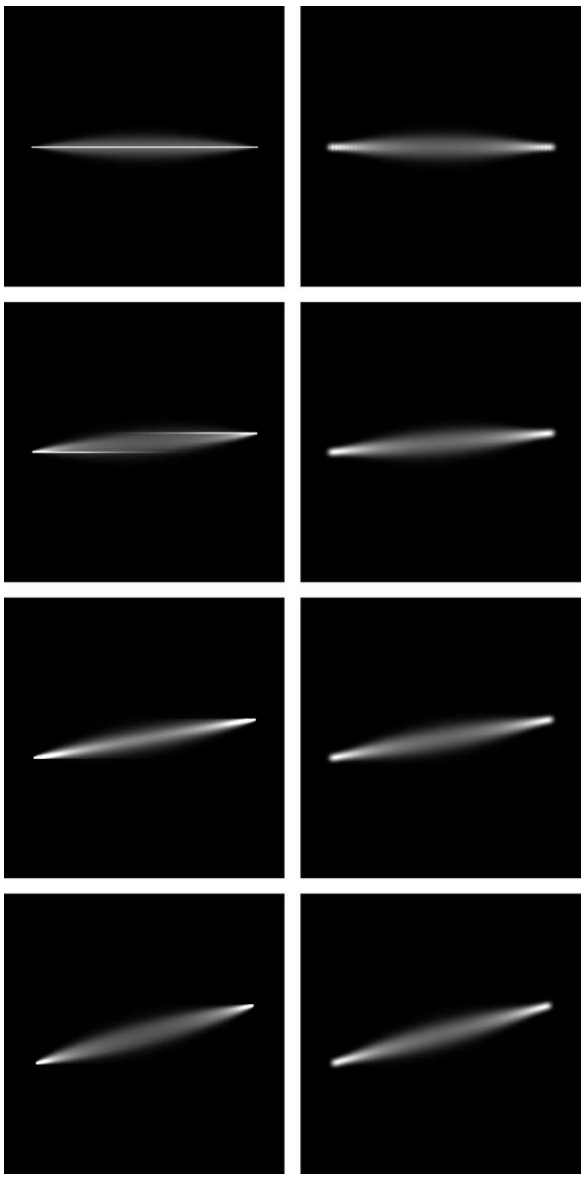

Figure 8. Straight line completion fields due to an initial stimulus consisting of two points on a circle with direction ϕ normal to the circle, with $\phi = 0^\circ, 5^\circ, 10^\circ, 15^\circ$. Left: Using the algorithm of [18]. Right: Using the new algorithm.

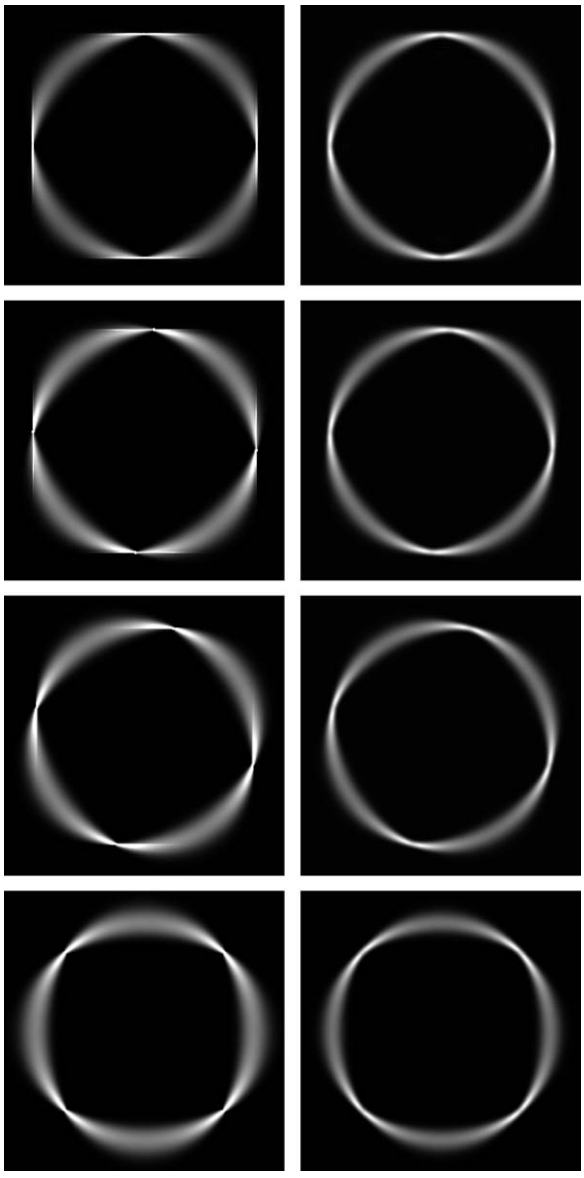

Figure 9. Completion fields due to rotations of the Ehrenstein initial stimulus in Fig. 1(a). From top to bottom, the initial conditions are rotated clockwise through angles, $\theta_0 = 0^\circ, 5^\circ, 15^\circ$ and 45°. Left: Using the algorithm of [18]. Right: Using the new algorithm.

completion fields due to rotations and translations of the Kanizsa Triangle stimulus in Fig. 1(b). Completion fields are shown in Fig. 2, which was discussed in the Introduction, and in Fig. 10. The top row of Fig. 10 shows completion fields due to the Kanizsa Triangle in Fig. 1(b). In the third row the initial conditions have been rotated clockwise by 5°. The second and fourth rows show the regions inside the boxes in the first and third rows, magnified 16 times. The completion fields computed using the method of Williams and Jacobs [18] were clipped above at 9×10^{-5}.

The completion fields in the right columns of Figs. 9 and 10, and in Fig. 2, demonstrate the Euclidean invariance of our new algorithm. This is in marked contrast

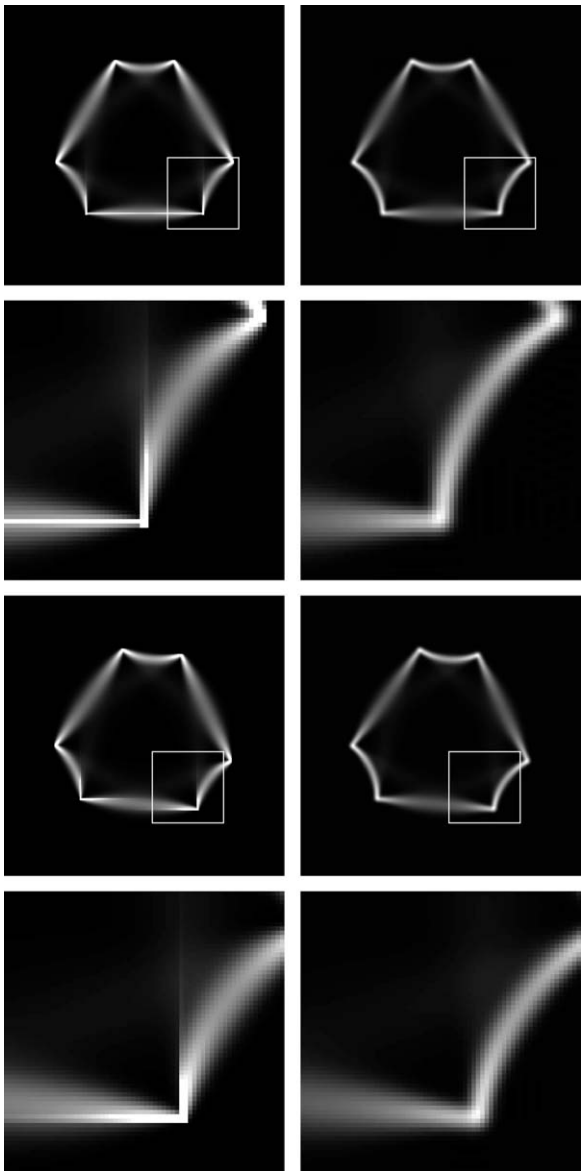

Figure 10. Top row: Completion fields due to the Kanizsa triangle initial stimulus in Fig. 1(b). Left: Using the algorithm of [18]. Right: Using the new algorithm. Second row: The regions inside the boxes, magnified 4×. Third row: Initial conditions rotated clockwise by 5°. Bottom row: The regions inside the boxes, magnified 4×.

with the obvious lack of Euclidean invariance in the completion fields in the left columns of Figs. 9 and 10. The visible straight line artifacts in these completion fields, which are oriented along the coordinate axes, are due to the anisotropic nature of the advection process in the algorithm of Williams and Jacobs [18], and (to a lesser extent), to the way in which the initial conditions were represented on the grid.

9. Conclusion

An important initial stage in the analysis of a scene requires completion of the boundaries of partially occluded objects. Williams and Jacobs introduced the notion of the stochastic completion field which measures the probability distribution of completed boundary shapes in a given scene. In this paper we have described a new algorithm for computing stochastic completion fields. As is required of any computational model of human visual information processing, our algorithm attempts to reconcile the apparent contradiction between the Euclidean invariance of human early visual computations on the one hand, and the observed sparseness of the discrete spatial sampling of the visual field by primary and secondary visual cortex on the other hand. The new algorithm reconciles these two contradictions by performing the computation in a basis of separable functions with spatial components similar to the receptive fields of simple cells in primary visual cortex. In particular, the Euclidean invariance of the computation is achieved by exploiting the shiftability and twistability of the basis functions.

In this paper, we have described three basic results. First, we have generalized Simoncelli et al.'s notion of shiftability and steerability in $\mathbf{R}^2$ to a more general notion of shiftability and twistability in $\mathbf{R}^2 \times S^1$. The notion of shiftability and twistability mirrors the coupling between the advection and diffusion terms in the Fokker-Planck equation, and at a deeper level, basic symmetries in the underlying random process characterizing the distribution of completion shapes. Second, we described a new method for numerical solution of the Fokker-Planck equation in a shiftable-twistable basis. Finally, we used this solution to compute stochastic completion fields, and demonstrated, both theoretically and experimentally, the invariance of our computation under translations and rotations of the input pattern.

Appendix

Proof of Proposition 2.1

First observe that, by Eq. (2.8),

$$T_{\vec{x}_0,\theta_0} P = \sum_{\vec{\ell},n} c_{\vec{\ell},n} T_{\vec{x}_0,\theta_0} \Psi_{\vec{\ell},n}, \tag{10.1}$$

and that the composition rule (2.11) for shift-twist transformations implies that

$$T_{\vec{x}_0,\theta_0}\Psi_{\vec{\ell},n} = T_{\vec{\ell}\Delta\vec{x}_0+R_{-n\Delta_\theta}(\vec{x}_0),\,\theta_0+n\Delta_\theta}\Psi. \tag{10.2}$$

The result now follows by applying the defining Eq. (2.6) for shiftability-twistability to express the right hand side of Eq. (10.2) in terms of the basis functions, $\Psi_{\vec{k},m}$, and then substituting the resulting equation into Eq. (10.1).

Proof of Proposition 2.2

For any $(\vec{x}_0, \theta_0) \in \mathbf{R}^2 \times S^1$,

$$\begin{aligned}
&\big(T_{\vec{x}_0,\theta_0}G_\omega\big)(\vec{x},\theta) \\
&\quad = g(R_\theta(\vec{x}-\vec{x}_0),\theta-\theta_0)\exp(i\omega(\theta-\theta_0)) && (10.3)\\
&\quad = \exp(-i\omega\theta_0)\,g(\vec{x}-\vec{x}_0)\exp(i\omega\theta) && (10.4)\\
&\quad = \exp(-i\omega\theta_0)\sum_{\vec{k}} b_{\vec{k}}(\vec{x}_0)(T_{\vec{k}\Delta,0}G_\omega)(\vec{x},\theta), && (10.5)
\end{aligned}$$

where (10.4) holds since $\|R_\theta\vec{x}-\vec{x}_0\| = \|\vec{x}-\vec{x}_0\|$, and (10.5) holds since g is effectively shiftable.

Analysis of the Accuracy and Shift-Twist Invariance of the Advection Process

In the continuum, the advection process is shift-twist invariant. Consequently, the greater the accuracy with which the continuous advection process (for time, Δt) is modeled by the discrete advection transformation, **A**, the greater the degree to which **A** is shift-twist invariant.

If the coefficient vector, $c_{\vec{k},\omega}$, evolves according to Eq. (5.10), then the the p.d.f., P, will advect in the continuum according to Eq. (5.7) provided that the basis, $\Psi_{\vec{k},\omega}$, is perfectly shiftable-twistable[19] and includes all (essentially) non-zero θ-frequencies of the interpolation functions, $b_{\vec{k}}(\Delta t[\cos\theta,\sin\theta]^{\mathrm{T}})$, and of the continuous solution, $P(\vec{x},\theta;t) = P(\vec{x}-t[\cos\theta,\sin\theta]^{\mathrm{T}},\theta;0)$, of the advection process.[20]

A numerical study showed that in the case that the initial p.d.f is a three-dimensional Gaussian, $P(\vec{x},\theta;0) = \exp(-\|\vec{x}\|^2/2\,\sigma_{\vec{x}}^2)\exp(-\theta^2/2\,\sigma_\theta^2)$, the number, N, of essentially non-zero θ-Fourier series coefficients of $P(\vec{x},\theta;t)$ is given by the formula

$$N = \frac{1}{\sigma_\theta}\left(\frac{at}{\sigma_{\vec{x}}}+b\right), \tag{10.6}$$

for some constants a and b. In particular if the spatial resolution of the initial conditions is increased by a factor of two in all three variables, then the number of frequencies, ω, must be multiplied by four to prevent aliasing in the advection process, and the number of spatial basis functions, $\psi_{\vec{k}}$, must also be multiplied by four to ensure that the basis is shiftable.

Proof of Proposition 5.2

The standard explicit finite difference scheme for the θ-diffusion of $P(\vec{x},\theta\,;t)$ on the grid of points, $\theta_n = n\Delta\theta$, where $n = 0, 1, ..., N-1$, is given by

$$\begin{aligned}
P(\vec{x},\theta_n;t+\Delta t) = {}& \lambda P(\vec{x},\theta_{n-1}\,;t)\\
&+(1-2\lambda)P(\vec{x},\theta_n\,;t)\\
&+\lambda P(\vec{x},\theta_{n+1}\,;t).
\end{aligned} \tag{10.7}$$

Substituting Eq. (10.7) into $P(\vec{x},\theta\,;t) = \sum_{\vec{k},\omega} c_{\vec{k},\omega}(t)\,\psi_{\vec{k}}(\vec{x})\exp(i\omega\theta)$ and equating coefficients of $\psi_{\vec{k}}$ yields the formula

$$\begin{aligned}
&\sum_\omega c_{\vec{k},\omega}(t+\Delta t)\exp(i\omega\theta_n)\\
&\quad = \sum_\omega c_{\vec{k},\omega}(t)\exp(i\omega\theta_n)[\lambda\exp(-i\omega\Delta\theta)\\
&\qquad +(1-2\lambda)+\lambda\exp(i\omega\Delta\theta)]
\end{aligned} \tag{10.8}$$

where we have used the fact that $\theta_{n+1} = \theta_n + \Delta\theta$. Equation (5.12) now follows by equating coefficients of $\exp(i\omega\theta_n)$.

The following argument shows that the diffusion transformation, **D**, is shift-twist invariant. First, a similar argument to the one just presented shows that Eq. (5.12) implies that

$$\begin{aligned}
P(\vec{x},\theta\,;t+\Delta t) = {}& \lambda P(\vec{x},\theta-\Delta\theta\,;t)\\
&+(1-2\lambda)P(\vec{x},\theta\,;t)\\
&+\lambda P(\vec{x},\theta+\Delta\theta\,;t)
\end{aligned} \tag{10.9}$$

for all $\theta \in S^1$. Equation (10.9) implies that $\mathbf{D}(T_{\vec{x}_0,\theta_0}P)(\vec{x},\theta)$ is given by

$$\begin{aligned}\lambda\big[&P\big(R_{\theta_0}(\vec{x}-\vec{x}_0),\theta-\theta_0-\Delta\theta;\,t+\Delta t\big)\\&+P\big(R_{\theta_0}(\vec{x}-\vec{x}_0),\theta-\theta_0+\Delta\theta;\,t+\Delta t\big)\big]\\&+(1-2\lambda)P\big(R_{\theta_0}(\vec{x}-\vec{x}_0),\theta-\theta_0;\,t+\Delta t\big)\end{aligned}$$

which is equal to $T_{\vec{x}_0,\theta_0}(\mathbf{D}P)(\vec{x}\,,\,\theta)$, i.e., $\mathbf{D}$ is shift-twist invariant.

Proof of Equation (6.1)

Equation (6.1) follows immediately from the two equations.

$$\begin{aligned}g_{\vec{k}}(\vec{x})\,g_{\vec{\ell}}(\vec{x}) = \frac{1}{2\widetilde{\nu}}\,\exp\left[-\left(\frac{\widetilde{\Delta}}{2\widetilde{\nu}}\|\vec{k}-\vec{\ell}\|\right)^2\right]\\ \times\widetilde{g}\left[\vec{x}-\frac{\widetilde{\Delta}}{\sqrt{2}}(\vec{k}+\vec{l})\right]\end{aligned}\tag{10.10}$$

and the shiftability formula

$$\widetilde{g}\left[\vec{x}-\frac{\widetilde{\Delta}}{\sqrt{2}}(\vec{k}+\vec{l})\right]=\sum_{\vec{j}}\widetilde{b}_{\vec{j}}\left[\frac{\widetilde{\Delta}}{\sqrt{2}}(\vec{k}+\vec{l})\right]\widetilde{g}_{\vec{j}}(\vec{x}).\tag{10.11}$$

To verify Eq. (10.10), observe that

$$\begin{aligned}&g_{\vec{k}}(\vec{x})\,g_{\vec{\ell}}(\vec{x})\\&\quad=\frac{1}{\nu^2}\exp[-(\|\vec{x}-\vec{k}\Delta\|^2+\|\vec{x}-\vec{\ell}\Delta\|^2)/2\nu^2],\end{aligned}\tag{10.12}$$

and that, by completing the square, $\|\vec{x}-\vec{k}\Delta\|^2+\|\vec{x}-\vec{\ell}\Delta\|^2=2\|\vec{x}-\frac{\Delta}{2}(\vec{k}+\vec{\ell})\|^2+\frac{\Delta^2}{2}\|\vec{k}-\vec{\ell}\|^2$.

Acknowledgments

The first author was partially supported by the Albuquerque High Performance Computing Center. The authors thank the reviewers for helping to improve the quality of the manuscript.

Notes

1. A discussion of this equation is provided in Section 3 below, see Eq. (3.1).
2. Although we allow the functions in visual computations to be complex valued, the input and output functions are defined to be the real parts of complex-valued functions.
3. We use this terminology even though the basis functions need not be linearly independent.
4. Periodic functions, ψ, are used in this definition (and in the definition of shiftable-twistable functions given below) simply to ensure that the number of basic shifts of ψ is finite.
5. The function, ψ, looks much more like the receptive field of a simple cell in primary visual cortex than does a Gaussian.
6. The θ-marginal, $\psi_{\vec{k},m}$ on $\mathbf{R}^2$, of the function, $\Psi_{\vec{k},m}$ on $\mathbf{R}^2\times S^1$, is similar in shape to the profile of a simple cell receptive field in primary visual cortex.
7. The factor $\exp(-i(\theta_0-m\Delta_\theta))$ steers $T_{\vec{0},\theta_0}\psi$ to $T_{\vec{0},m\Delta_\theta}\psi$.
8. The Gabor function is often used to model two-dimensional simple cell receptive fields in primary visual cortex [7].
9. Nor are we blameless in this respect. Williams and Jacobs [17, 18] used 36 directions (including 0°, 60° and 120°) and demonstrated their computation with a Kanizsa Triangle with sides of 0°, 60° and 120° orientation.
10. The need to use a slightly different basis to represent completion fields is not biologically implausible, since the experimental evidence described in [20] suggests that the neural locus of the source and sink fields could be primary visual cortex, while completion fields are more likely located in secondary visual cortex.
11. The parameterization of the helix is $x(s)=t\cos s$, $y(s)=t\sin s$, $\theta(s)=s$, where $0\le s\le 2\pi$.
12. Note that this simple scaling result does *not* imply that if the spatial resolution of the initial conditions is increased by a factor of two, that sixteen times as many basis functions are required to represent the source field. In fact, because the diffusion operator attenuates high frequencies, only about eight times as many basis functions are required.
13. If the transformations, $\mathbf{A}$ and $\mathbf{D}$, are shift-twist invariant, then so is $\mathbf{A}\circ\mathbf{D}$.
14. The interpolation functions $\widetilde{b}_{\vec{j}}$ are evaluated at $\frac{\widetilde{\Delta}}{\sqrt{2}}(\vec{k}+\vec{\ell})=\frac{\Delta}{2}(\vec{k}+\vec{\ell})$, since $G_{\vec{k},\omega}G_{\vec{\ell},\eta}$ is a Gaussian centered at $\frac{\Delta}{2}(\vec{k}+\vec{\ell})$.
15. The rationale for this method of calculating the source field is that, for each fixed θ, the Fokker-Planck equation is a constant coefficient linear equation.
16. The diffusion parameter, σ, was required to be larger in the last experiment because of the high curvature circles in the Kanizsa triangle.
17. The angles, ϕ, were taken in 5° increments from 0° to 45°. For illustration purposes the ϕ-axis was extended to 360° so as to reflect the symmetry of the grid. Both graphs were normalized to have average value one.
18. Because of the periodicity in the spatial variables, $\vec{x}$, to avoid wrap around in this experiment, for the new algorithm the computation was performed on a $80.0\times 80.0\times 2\pi$ space with $K=320$.
19. Since the basis functions are only effectively shiftable-twistable, there is inevitably some error in the advection process. This error is not Euclidean invariant.
20. For small $\Delta t\approx 0.1$, the number of nonzero θ-frequencies of the interpolation functions is much less than that of P.

References

1. P.C. Bressloff, J.D. Cowan, M. Golubitsky, P. Thomas, and M. Wiener, "Geometric visual hallucinations, Euclidean symmetry, and the functional architecture of striate cortex," *Phil. Trans. Roy. Soc. (Lond.)*, Vol. B 356, pp. 1–32, 2001.

2. I. Daubechies, *Ten Lectures on Wavelets*, SIAM: Philadelphia, 1992.
3. J. Daugman, "Complete discrete 2-D Gabor transforms by neural networks for image analysis and compression," *IEEE Trans. Acoustics, Speech, and Signal Processing*, Vol. 36, No. 7, pp. 1,169–1,179, 1988.
4. W. Freeman and E. Adelson, "The design and use of steerable filters," *IEEE Transactions on Pattern Analysis and Machine Intelligence*, Vol. 13, No. 9, pp. 891–906, 1991.
5. S. Grossberg and E. Mingolla, "Neural dynamics of form perception: Boundary completion, illusory figures, and neon color spreading," *Psychological Review*, Vol. 92, pp. 173–211, 1985.
6. R. Heitger and R. von der Heydt, "A computational model of neural contour processing, figure-ground and illusory contours," in *Proc. of 4th Intl. Conf. on Computer Vision*, Berlin, Germany, 1993.
7. T.S. Lee, "Image representation using 2D Gabor wavelets," *IEEE Transactions on Pattern Analysis and Machine Intelligence*, Vol. 18, No. 10, pp. 959–971, 1996.
8. Z. Li, "A neural model of contour integration in primary visual cortex," *Neural Computation*, Vol. 10, No. 4, pp. 903–940, 1998.
9. D. Mumford, "Elastica and computer vision," in *Algebraic Geometry and Its Applications*, Chandrajit Bajaj (Ed.), Springer-Verlag: New York, 1994.
10. P. Parent and S.W. Zucker, "Trace inference, curvature consistency and curve detection," *IEEE Transactions on Pattern Analysis and Machine Intelligence*, Vol. 11, No. 8, pp. 823–889, 1989.
11. M. Porat and Y. Zeevi, "The generalized Gabor scheme of image representation in biological and machine vision," *IEEE Transactions on Pattern Analysis and Machine Intelligence*, Vol. 10, No. 4, pp. 452–468, 1988.
12. A. Shashua and S. Ullman, "Structural saliency: The detection of globally salient structures using a locally connected network, *2nd Intl. Conf. on Computer Vision*, Clearwater, FL, 1988, pp. 321–327.
13. E. Simoncelli and H. Farid, "Steerable wedge filters for local orientation analysis," *IEEE Trans. Image Proc.*, Vol. 5, No. 9, pp. 1377–1382, 1996.
14. E. Simoncelli, W. Freeman, E. Adelson, and D. Heeger, "Shiftable multiscale transforms," *IEEE Trans. Information Theory*, Vol. 38, No. 2, pp. 587–607, 1992.
15. K.K. Thornber and L.R. Williams, "Analytic solution of stochastic completion fields," *Biological Cybernetics*, Vol. 75, pp. 141–151, 1996.
16. B.A. Wandell, *Foundations of Vision*, Sinauer Press, 1995.
17. L.R. Williams and D.W. Jacobs, "Stochastic completion fields: A neural model of illusory contour shape and salience," *Neural Computation*, Vol. 9, No. 4, pp. 837–858, 1997.
18. L.R. Williams and D.W. Jacobs, "Local parallel computation of stochastic completion fields," *Neural Computation*, Vol. 9, No. 4, pp. 859–881, 1997.
19. L.R. Williams and K.K. Thornber, "Orientation, scale and discontinuity as emergent properties of illusory contour shape," *Neural Computation*, Vol. 13, No. 8, pp. 1683–1711, 2001.
20. L.R. Williams and J.W. Zweck, "A rotation and translation invariant discrete saliency network," *Biological Cybernetics*, Vol. 88, No. 1, pp. 2–10, 2003.
21. L.R. Williams, J. Zweck, T. Wang, and K.K. Thornber, "Computing stochastic completion fields in linear time using a resolution pyramid," *Computer Vision and Image Understanding*, Vol. 76, No. 3, pp. 289–297, 1999.
22. S. Yen and L. Finkel, "Salient contour extraction by temporal binding in a cortically-based network," *Neural Information Processing Systems*, Vol. 9, Denver, CO, 1996.

John Zweck received a Ph.D. in pure mathematics from Rice University in 1993. After graduating, he continued his research in differential geometry and geometric analysis in mathematics departments at Rice University, The University of New York at Stony Brook, The University of Nevada Reno and The University of Texas at Austin. From 1998-2000 his research on human and computer vision in the Computer Science Department at the University of New Mexico focused on numerical algorithms for visual computations. In 2000 he became a Research Associate in the Computer Science and Electrical Engineering Department at the University of Maryland Baltimore County (UMBC), where he does analysis and numerical simulation of optical fiber communications systems. In Fall 2003 he will commence a position as an Assistant Professor in the Department of Mathematics and Statistics at UMBC.

Lance R. Williams received the B.S. degree in computer science from the Pennsylvania State University in 1985 and the M.S. and Ph.D. degrees in computer science from the University of Massachusetts at Amherst in 1988 and 1994, respectively. He spent four years as a post-doctoral scientist at NEC Research Institute. He is now an associate professor in the Computer Science Department at the University of New Mexico in Albuquerque. His principal research interests are human visual information processing, perceptual organization for artificial vision systems, and neural computation.